ELECTRICAL, MAGNETIC AND THERMAL PROPERTIES OF UNi_2Si_2 AND UNi_2Ge_2

By

Yuebin Ning, B.Sc., M.Sc.

A Thesis

Submitted to the School of Graduate Studies

in Partial Fulfilment of the Requirements

for the Degree Doctor of Philosophy

McMaster University

June 1991

DOCTOR OF PHILOSOPHY (1991) McMASTER UNIVERSITY

(Physics) *Hamilton, Ontario*

TITLE: Electrical, Magnetic and Thermal Properties of UNi_2Si_2 and UNi_2Ge_2

AUTHOR: Yuebin Ning, B.Sc. (*Jilin University, PRC*)
M.Sc. (*University of Alberta*)

SUPERVISOR: Professor W. R. Datars

PAGES: *ix*, 97

ABSTRACT

The magnetic susceptibility, resistivity, and Hall coefficient of single crystals of UNi_2Si_2 and UNi_2Ge_2 have been investigated. Thermoelectric power and specific heat measurements of UNi_2Si_2 have also been carried out.

The magnetic susceptibility of UNi_2Si_2 and UNi_2Ge_2 follows the Curie-Weiss law in the paramagnetic state at high temperatures and the anisotropy shows that the magnetic moments on the U atoms are constrained to lie preferentially along the c axis.

The resistivity of these two compounds is largely due to magnetic scattering and the phonon contribution only amounts to 8-14% of the total resistivity at room temperature. Along the c axis, the resistivity shows a Kondo type of behaviour at high temperatures. The temperature dependence of the Hall coefficient can be accounted for by a theoretical model invoking a magnetic skew-scattering process. Distinct features and anomalies are observed in both the resistivity and the Hall coefficient at the magnetic transitions of these two compounds.

The thermoelectric power of single crystal UNi_2Si_2 is also anisotropic, with the c-axis component strongly coupled to the magnetic phase transitions. The gamma value obtained from the specific heat measurements of UNi_2Si_2 is 22 mJ mol^{-1} K^{-2} which indicates a small mass enhancement in the system.

ACKNOWLEDGEMENTS

I wish to express my gratitude to my research supervisor, Dr. W. R. Datars, for his continued help, encouragement and advice throughout the course of this research.

Special thanks are due to Dr. C. V. Stager for the beautiful magnetization measurements and many helpful discussions of magnetic properties in general, to Mr. A. Ler Dawson for the specific heat measurements, and to Dr. J. P. Carbotte for discussions of the heavy fermion materials. I am grateful to Miss H. Lin and Dr. M. F. Collins for sharing their neutron results prior to publication and also for many valuable discussions. Many thanks to Mr. T. Olech for his technical assistance, and to Mr. W. Scott for his unflagging effort in producing large quantities of liquid helium. I would like to thank Mr. C. G. Trendall and Mr. F. A. Hegmann for their generous help in various aspects. I would also like to thank Mr. J. D. Garrett for providing high quality single crystal samples, without which the experiment would never have been born.

Finally, I would like to thank my wife Yan for her support during the final phase of my graduate career and her understanding of long working hours.

TABLE OF CONTENTS

LIST OF TABLES

LIST OF FIGURES

CHAPTER 1

INTRODUCTION

In recent years, there has been a great amount of interest in the class of materials RT_2X_2, where R is either the rare earth element Ce or the actinide element U, T is a transition metal and X is either Si or Ge. Although most of these compounds crystallize in the same $ThCr_2Si_2$ type of body centred tetragonal structure, they exhibit a variety of properties, including heavy fermion behaviour, magnetic ordering, superconductivity and enhanced Pauli paramagnetism. Systematic studies (Palstra, 1986) of the 1-2-2 compounds of RT_2Si_2 indicate that those with a transition metal that has a small number of d-electrons are commonly Pauli paramagnetic, those with an intermediate number of d-electrons usually result in a heavy-fermion state and those with a large number of d-electrons are likely to result in systems which order magnetically. A similar trend has also been established in the UT_2Ge_2 compounds (Dirkmaat, 1989).

From these systematic studies, a phenomenological description of the band structure has emerged. The model is composed of a very broad conduction band and a narrow band which is related to the atomic f-levels of the Ce or U atoms.

The idea is that as one moves towards the heavier transition metals (hence more d electrons), the Fermi energy increases. When the narrow band lies above the fermi level, there is no local magnetic moment. If the narrow band is at the Fermi level, the narrowness of the band leads to a large specific heat and a heavy-fermion state at low temperatures. When the narrow band lies below the Fermi level, it is filled, and there is the formation of a localized moment at the cerium or uranium site.

Among these three groups of materials, one group has attracted particular attention for the past several years, namely the heavy-fermion materials. A unique feature of the heavy-fermion materials is the heaviness of the charge carriers in the system. In usual metals, the specific heat at low temperatures contains a linear term due to the charge carriers and a cubic term from lattice vibrations (Ashcroft and Mermin, 1976):

$$c_p(T) = \gamma T + \beta T^3 \qquad (1.1)$$

For a free electron metal such as Cu, the γ value is only 0.7 mJ mol^{-1} K^{-2}. For the heavy-fermion metals however, γ values of several hundred mJ mol^{-1} K^{-2} are fairly common. A direct implication of the large γ values is the large effective mass m^* (Stewart, 1984; Coles, 1987) associated with the charge carriers in the heavy-fermion metals. A striking feature of the heavy-fermion metals is the development of the so called "coherent state" (Lee et al, 1987; Coles, 1988) at low

temperatures, in which the resistivity decreases dramatically with decreasing temperature due to the "coherent" nature of the scattering. One other aspect of the heavy-fermion puzzle is the fact that some of the large-γ compounds are superconductors at low temperatures. Since it was generally accepted that good local moments and spin-fluctuations are destructive to the standard BCS type superconductivity (s-wave pairing), much effort has been made to identify the nature of the pairing in heavy-fermion superconductors. Despite intense efforts, much of the puzzle of the heavy-fermion state remains unsolved and a formal theoretical treatment providing a consistent picture for all the aspects has yet to emerge. On the other hand, it has become apparent through the phenomenological description given above that all the three groups are ultimately connected. One would be naive to single out the heavy-fermion state from the rest which obviously contain much needed further information for solving the puzzle.

UNi_2Si_2 and UNi_2Ge_2 are among those compounds which become magnetically ordered at low temperatures. The rich magnetism in these magnetically ordered materials forms a broad and interesting subject in its own right. However, it is hoped that detailed studies of these compounds may also shed new light on many closely related problems, particularly those of the heavy-fermion state. Like many of the materials in the RT_2X_2 class, these two compounds also crystallize in the

tetragonal $ThCr_2Si_2$ type of structure, with the atomic arrangement shown in Figure 1.1. The space group of the structure is I4/mmm. The uranium atoms occupy the 2a positions to form a simple body-centered tetragonal sublattice. The nickel atoms are in the 4d positions and the silicon or germanium atoms are located at the 4e positions. The lattice parameter a is typically around 4 Å and the lattice parameter c is about 9.5 Å.

Because of the anisotropy in the crystal structure, this class of materials exhibits strong anisotropies in many of the physical properties. The magnetism of these materials are associated primarily with the Ce or U atoms although, occasionally, moments are also present on the transition metal sites. In nearly all of the magnetic susceptibility measurements of single crystal samples that have been reported, the susceptibility along the c axis is larger than the susceptibility perpendicular to the c axis in the paramagnetic state. Most of the magnetically ordered compounds are found to have the magnetic moments aligned along the tetragonal c axis in their ordered states. Since the conduction electrons are strongly correlated with the localized f electrons, such magnetic anisotropy has a profound influence upon the transport properties in the systems.

For the entire class of RT_2X_2 compounds, the transport properties are, to a very large extent, determined by magnetic scattering of the conduction electrons. The resistivity of

Figure 1.1

The body-centered tetragonal crystal structure of UNi_2Si_2 and UNi_2Ge_2. X represents either Si or Ge.

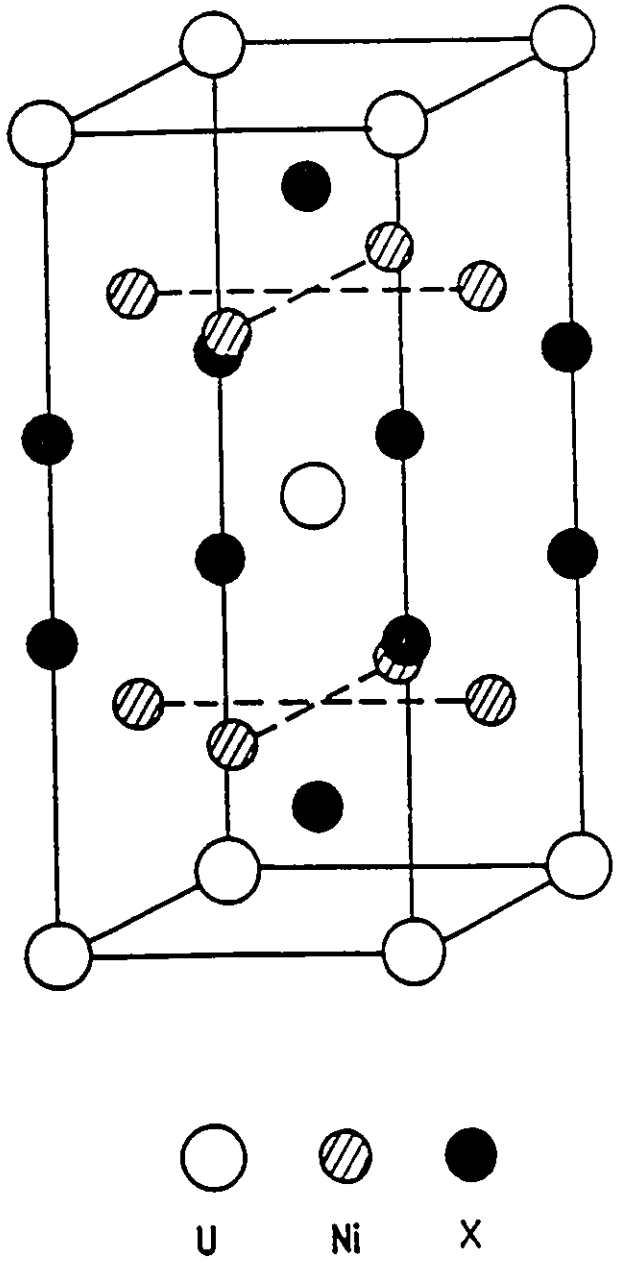
U
Ni
X

these compounds is often in the hundreds of $\mu\Omega$ cm at room temperature, and often shows a Kondo type of behaviour before the coherent state or magnetic ordering sets in. Among the existing single crystal measurements, a consistent trend seems to be that the Kondo increase of resistivity with decreasing temperature is likely to occur along the tetragonal c axis if not for all the crystal axes. For those which order magnetically, spin-wave (magnon) scattering at low temperatures is of importance. Detailed analysis of the resistivity measurements at low temperatures should provide useful information about electron-magnon coupling and the magnon excitation spectrum in the system. The Hall coefficient of these compounds is often positive and much larger than in normal metals. In general, the Hall coefficient contains an ordinary component due to the Lorentz force and an anomalous component from magnetic skew scattering. The thermoelectric power in these materials is much like that in the transition metals and rare earths (Blatt et al, 1976), large in magnitude and complex in nature, but nevertheless is useful in supplementing information about the transport anisotropy and energy scale (Amato et al, 1989) of these systems. Because of the strong interaction between the conduction electrons and the localized magnetic moments, the transport properties often show anomalous behaviour at the magnetic ordering temperature. Closer examinations of these anomalies usually provide valuable information about the ordered state and the

renormalization of the Fermi surface. In particular, these features at the transition temperatures can be monitored under pressure or in a magnetic field to map out the phase diagrams, providing further insight into the mechanism of the magnetic interaction.

In Chapter 2, a brief account of the theoretical background will be presented. In Chapter 3, the experimental techniques and apparatus employed in this study are summarized. Chapter 4 & 5 present the experimental results of UNi_2Si_2 and UNi_2Ge_2 along with a detailed discussion. Finally, Chapter 6 provides the summary and the conclusions of the study.

CHAPTER 2

THEORETICAL BACKGROUND

A Magnetic Susceptibility

2.1 The Curie-Weiss Law

In the paramagnetic state of a system of localized magnetic moments (magnetic ions), the molar magnetic susceptibility χ, defined as M/H where M is the magnetization per mole and H the applied magnetic field, is expected to obey the Curie law:

$$\chi = C/T \qquad (2.1)$$

provided that there is no coupling between the moments. The constant C is called the Curie constant and is given by:

$$C = \frac{N_A (p\mu_B)^2}{3k_B} \qquad (2.2)$$

where N_A is the number of ions with magnetic moments per mole, μ_B is the Bohr magneton and p the effective number of Bohr magnetons per magnetic ion. However, when there is an interaction between the magnetic ions, the moments will tend to align themselves in a certain way. We first consider the case of the ferromagnetic interaction in which the moments

tend to align parallel to each other. The interaction is treated as an effective magnetic field acting on a given individual moment and is assumed to be proportional to the magnetization:

$$H_{Eff} = \lambda M \tag{2.3}$$

so that with an applied field H_a, the total magnetization is given by:

$$M = \chi(H_a + \lambda M) \tag{2.4}$$

which yields the Curie-Weiss law:

$$\chi = M/H_a = C/(T-\lambda C) \tag{2.5}$$

where C is given by (2.2). This expression describes fairly well the observed susceptibility in the paramagnetic region above the magnetic ordering temperature (Curie point).

For the case of the antiferromagnetic interaction, the situation is slightly different: instead of aligning parallel to each other, the magnetic moments tend to align antiparallel to each other in an antiferromagnetic arrangement. Treating the system as two sub-lattices A and B and introducing an antiparallel interaction between sites A and B, one can show that the susceptibility in the paramagnetic region of an antiferromagnet above the ordering temperature (Néel point) obeys the following expression (Kittel, 1976):

$$\chi = C/(T + T_N) \tag{2.6}$$

where T_N is the Néel temperature and C is a constant given by the expression of (2.2). The above expression was derived assuming a nearest-neighbour interaction. Experimental results

above T_N are of the form:

$$\chi = C/(T + \theta) \qquad (2.7)$$

where θ differs from T_N. The difference can be largely resolved if the next-nearest-neighbour interaction is also considered (Kittel, 1976).

In practice, the expressions (2.5) and (2.7) are generalized into:

$$\chi = C/(T-\theta_{CW}) \qquad (2.8)$$

with positive values of θ_{CW} (Curie-Weiss temperature) for ferromagnetic coupling and negative values of θ_{CW} for the case of antiferromagnetic coupling. In addition, the inverse of χ is often plotted against T to check the validity of the Curie-Weiss law and to extrapolate the values of θ_{CW} and C which in turn gives the effective magnetic moment per ion $p\mu_B$.

B Electrical Resistivity:

2.2 The Ideal Resistivity

In normal metals, the electrical resistivity can be written as $\rho = m/ne^2\tau$ where m is the band mass of the charge carrier and n the density. $1/\tau$ is the scattering probability of the Bloch waves and is the factor which leads to the temperature dependence of the resistivity. For a simple non-magnetic metal, the temperature dependence of the resistivity is entirely due to the scattering of conduction electrons with phonons. This resistivity (often called the "ideal" or

"intrinsic" resistivity), together with the impurity scattering resistivity, makes up the total resistivity:

$$\rho(T) = \rho_o + \rho_i \qquad (2.9)$$

where ρ_o is the residual resistivity and ρ_i is the ideal resistivity which is described by the Gruneisen-Bloch expression (Gruneisen, 1933):

$$\rho_i = \frac{C}{\theta_D}\left(\frac{T}{\theta_D}\right)^5 \int_0^{\theta_D/T} \frac{x^5 dx}{(e^x-1)(1-e^{-x})} \qquad (2.10)$$

where C is a constant and θ_D the characteristic temperature (Debye temperature) of the lattice above which all the phonon modes begin to be excited. For temperatures well above or below the Debye temperature θ_D, the expression of the total resistivity reduces to:

$$\rho = \rho_o + AT^5 \qquad T << \theta_D \qquad (2.11)$$

$$\rho = \rho_o + BT \qquad T >> \theta_D \qquad (2.12)$$

2.3 The Kondo Effect And Kondo Systems

In metals with dilute magnetic impurities, the resistivity at low temperatures often rises with decreasing temperature and leaves a resistance minimum at temperatures where normal $\rho_T \sim T^5$ metallic behaviour is expected. This phenomenon is known as the Kondo effect and is caused by the exchange interaction between the conduction electrons and the localized magnetic moments on the impurity sites. The

scattering process is basically a "spin-flip" process in which the conduction electrons flip their spins to "compensate" the localised impurity moments. The first theoretical account of this effect was due to Kondo (Kondo, 1964). The starting point of Kondo's treatment is a single isolated magnetic impurity in the otherwise non-magnetic host metal. It is assumed further that the interaction between a conduction electron and the magnetic impurity is the "s-d" exchange interaction of the following form:

$$H = -J\sigma.S \qquad (2.13)$$

where J is the s-d exchange integral (s here represents the conduction or s-electron and d the localised d or f-electron of the impurity), σ and S are the spins of the conduction electron and the magnetic impurity, respectively. By including the second order terms in the scattering probability, Kondo found that the resistivity due to this scattering process exhibits a logarithmic temperature dependence:

$$\rho(T) = \rho_o - \rho_k \ln T \qquad (2.14)$$

where ρ_o and ρ_k are positive constants and the sign of J is assumed to be negative (antiferromagnetic exchange). The above expression leads to an increasing resistivity with decreasing temperature and is valid above the characteristic "Kondo temperature" T_K. Here, $k_B T_K$ is the binding energy of this antiparallel spin alignment. Because of this Kondo effect, metals with dilute (concentrated) magnetic impurities are also called dilute (concentrated) Kondo systems. If the magnetic

ions are arranged periodically, then the systems are called Kondo lattices. Although Kondo scattering process was originated for the single impurity problem, it has been shown experimentally that, the Kondo scattering also contributes an important part to the resistivity of the Kondo lattice systems at high temperatures where the scatterings become independent of each other (Schoenes et al, 1987; Coles et al, 1987).

2.4 Spin-Wave And Spin-Disorder Scattering

At the absolute zero of temperature, the magnetic moments in a ferromagnetic or antiferromagnetic metal are all aligned and the system becomes an ordered array of magnetic moments. If there were no impurity, then conduction electrons with either spin could propagate through this perfectly periodic lattice without being scattered incoherently. There would be thus no resistivity.

As the temperature is raised, thermal excitations, both magnetic and vibrational, will occur. Here we concentrate on those of magnetic origin. The magnetic excitations of the lowest energy, which are hence the first to be excited, are spin waves or magnons. These are the collective excitations of the aligned spins, just like phonons in the case of lattice vibrations. At high enough temperatures, where more thermal energy is available, individual ions can have their spin orientations disturbed randomly by the thermal fluctuations, and it is more

appropriate to treat the scattering process as spin-disorder scattering. The influence of these excitations on resistivity will be discussed below.

We first consider the electrical resistivity from spin-wave scattering. We restrict ourselves to the low temperature region since it is only at low temperatures that scattering due to magnons predominates. The formal treatment of magnon scattering has been carried out by Andersen and his coworkers (Andersen et al, 1976, 1979). The general expression for magnon resistivity ρ_m is the following:

$$\rho_m = A \int_0^{2k_F} \left(\frac{1}{2k_F}\right)^4 q^3 dq \int \frac{d\Omega}{4\pi} |g_q|^2 \frac{\hbar\omega/k_B T}{\sinh^2(\hbar\omega/2k_B T)} \qquad (2.15)$$

where $A=3\pi m/(e^2\hbar\varepsilon_F)$, $|g_q|$ is the electron-magnon coupling constant and $\hbar\omega$ the energy of a magnon which is a function of the wave vector **q**.

For a simple ferromagnet, the dispersion relation of magnons at low temperatures is simply $\hbar\omega = Cq^2$ where C is a constant, and the coupling constant $|g_q|$ is independent of **q**. Inserting these into expression (2.15), one arrives at a T^2 dependence of the magnon resistivity for a ferromagnet. In the case of a simple antiferromagnet, $\hbar\omega = Dq$ where D is again a constant and $|g_q| \propto q$. The expression (2.15) gives a T^5 dependence for the magnon resistivity at low temperatures.

If there is magnetic anisotropy in the system,

however, an energy gap will be present in the dispersion of magnons, as in the case of URu_2Si_2 and many other uranium ternary compounds. For an isotropic magnet, the lowest energy of a magnon is zero which corresponds to a free rotation of the completely ordered spin configuration (q=0). In the case of an anisotropic magnet, such a rotation costs a certain amount of energy, so that there is a minimum amount of energy (gap energy) required to create a magnon. At low temperatures (small q limit), the dispersion relation can be expanded around its minimum which is simply:

$$\hbar\omega = \Delta + cq^2 \qquad (2.16)$$

where Δ is the energy gap in the magnon spectrum and c a constant. The coupling constant in this case is again independent of the momentum transfer q. Inserting (2.16) into the expression for the magnon resistivity, one can show that the resistivity due to the scattering of gapped magnons is of the form (Andersen et al, 1979):

$$\rho_m \propto \frac{T}{\Delta}[1+2\frac{T}{\Delta}]\exp(-\Delta/T) \qquad (2.17)$$

At higher temperatures, ions may have their spin orientations disturbed individually by the thermal fluctuations and the excitations are no longer collective in nature (Dugdale, 1976). Let us consider a simple case in which the magnetic moment of one particular ion is "flipped" over from its direction in the ordered state. Via the s-d exchange interaction, conduction electrons propagating through this

disordered spin will be scattered which results in additional resistivity. As the temperature becomes higher, more and more such spin-disorders occur and the contribution to resistivity becomes progressively larger. Above the Curie or Néel temperature, the spin orientations become completely disordered and the resistivity due to spin-disorder scattering eventually saturates and becomes independent of temperature.

2.5 Spin-Fluctuation Scattering And Magnetic Superzone

In a magnetic metal just above the ordering temperature, there are long-lived fluctuations in which the spins in a region of the metal are aligned just as in the ordered state. Similarly, there should also be regions of non-ordered paramagnetic state fluctuating in the ordered state just below the magnetic ordering temperature (Dugdale, 1976). These spin fluctuations scatter the conduction electrons and bring about anomalous behaviours in the resistivity. Since these spin fluctuations are only important near the magnetic critical point (Richard and Geldert, 1977; Alexander et al, 1976), they are also called "critical scattering". In addition to the critical scattering, there is also the gapping effect in an antiferromagnet, due to the formation of a magnetic superzone below the Néel temperature (assuming that the magnetic superzone intersects with the Fermi surface). The term "superzone" comes about as the magnetic periodicity may well be different from the lattice periodicity, producing a

"magnetic" Brillouin zone in addition to the "lattice" one. We first discuss the contribution due to the critical scattering.

The treatment of spin fluctuation scattering is a rather complicated subject and a detailed account is beyond the scope of the thesis. Instead, we shall discuss rather briefly and qualitatively the basic approach involved and the important results derived from it. The starting point is again the s-d exchange interaction between the conduction electrons (s) and the localized d or f electrons. The first theoretical study of spin-fluctuation scattering in antiferromagnets was by Suezaki and Mori (Suezaki and Mori, 1969) and later, but independently, by Geldart and Richard (Geldart and Richard, 1972). Here we simply follow the line of Suezaki and Mori. The model hamiltonian of the system they used is the following:

$$H = H_s + H_d + H_{s-d} \tag{2.18}$$

where H_s is the hamiltonian of the s electrons, H_d of the d or f (localized) electrons and H_{s-d} of the mixing of s and d or f electrons. Their expressions are given as:

$$H_s = \sum_{q\sigma} \epsilon_q a^+_{q\sigma} a_{q\sigma} \qquad (\epsilon_q = \hbar^2 q^2/2m) \tag{2.19}$$

$$H_d = -N^{-1} \sum_k J_k S_k \cdot S_{-k} \qquad (S_k = \sum_{j=1}^{N} e^{ik\cdot R} S_j) \tag{2.20}$$

$$H_{s-d} = -N^{-1}\sum_{q}\sum_{q'} I_{q-q'}\{(a^{+}_{q'+}a_{q+} - a^{+}_{q'-}a_{q-})S^{z}_{q-q'}$$

$$+ a^{+}_{q'-}a_{q+}S^{+}_{q-q'} + a^{+}_{q'+}a_{q-}S^{-}_{q-q'}\} \qquad (2.21)$$

where $a_{q\sigma}$ and $a^{+}_{q\sigma}$ are respectively the annihilation and creation operators of conduction electrons with wave vector q and spin σ, and S_k is the spin operator of the d or f electrons with wave vector **k**. J_k is the exchange constant. The electron-phonon interaction is omitted since the primary interest here is the scattering by fluctuations of the localized spins in the vicinity of the magnetic ordering temperature.

Using the notation of the creation and annihilation operators, the current operator can be written as:

$$J_{\mu} = -(\frac{e}{m})\sum_{q\sigma}\hbar q_{\mu}a^{+}_{q\sigma}a_{q\sigma} \qquad (2.22)$$

where μ represents any of the coordinates x, y or z.

Using the above model hamiltonian and current operator, and following the general linear response formula, they were able to derive the following expression for the derivative of the resistivity due to spin-fluctuation scattering, in the vicinity of the Néel temperature T_N:

$$\frac{d\rho_{\mu\nu}}{dT} \approx \mp B_{\pm}t^{-\lambda} \qquad (2.23)$$

where $t=|T-T_N|/T_N$ is the reduced temperature, λ is the critical exponent and $B_\pm$ is a constant factor. The factor $-B_+$ is for the case $T > T_N$ and the factor $+B_-$ is for $T < T_N$. It is worth pointing out that, because of the assumption made in deriving equation (2.23), the expression is only valid for resistivity along the direction of **K** where **K** is the magnetic reciprocal lattice vector. For resistivity perpendicular to **K**, the anomaly in $d\rho/dT$ is expected to be the same as in the ferromagnets which we shall discuss later.

As we mentioned earlier, in addition to the spin-fluctuation scattering term, there is also the gapping effect below T_N if the magnetic Brillouin zone intersects with the fermi surface. That is, the conduction electrons will feel a new magnetic potential whose period is $2\pi/K$ besides the usual lattice potential. The new potential produces band gaps as is shown schematically in Figure 2.1a. The formation of a gap leads to a reduction of the effective number of conduction electrons along the **K** direction. This in turn will lead to a sharp increase in resistivity. The effective number of conduction electrons along the **K** direction was first derived by Miwa (Miwa, 1963) and can be written:

$$n'_{eff} = n\{1-(3\pi/8)(\Delta/\epsilon_F)(K/q_F)\} \qquad (2.24)$$

where Δ is the energy gap, $\epsilon_F=1/2\hbar q_F^2$ the Fermi energy, n the number of conduction electrons per unit volume before the formation of the gap. The temperature dependence comes from the energy gap Δ. Combining the gap effect and the spin-

Figure 2.1

(a) Schematic diagram of the Fermi surface with the energy gaps produced by the magnetic ordering potential.
(b) Predicted resistivity behaviour just below T_N parallel to the direction of **K**.

(a)

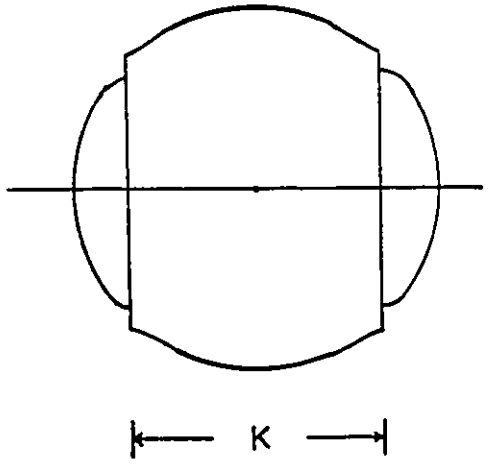

(b)

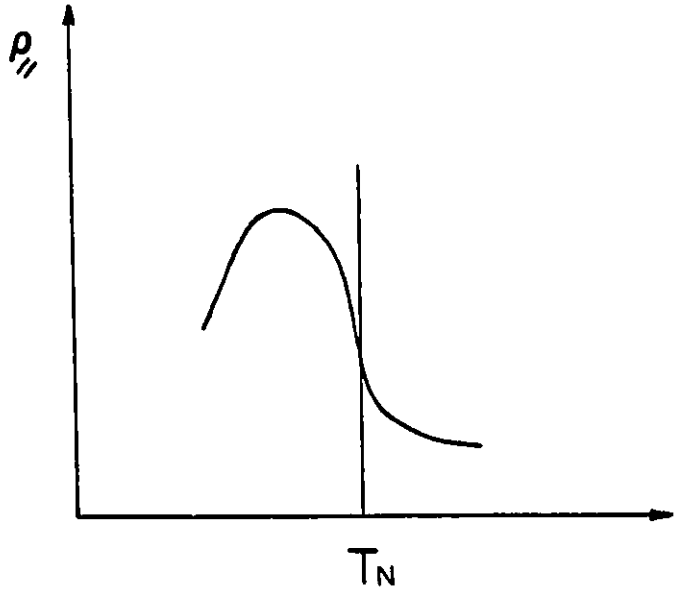

fluctuation scattering, we finally arrive at the expression of the resistivity derivative along the K direction below the Néel temperature T_N (Suezaki and Mori, 1969):

$$d\rho'/dT = -B_g t^{-(1+\lambda)/2} + B_- t^{-\lambda} \qquad (T<T_N) \qquad (2.25)$$

where the first term with the constant B_g is due to the formation of an energy gap and the second term is due to spin-fluctuation scattering from equation (2.23). Through the scaling relation, one can generally show that $(1+\lambda)/2 > \lambda$. Therefore, the first term of (2.25) would always have a stronger divergence than the second one. In the case of $B_- > B_g$, we thus expect the resistivity $\rho_\parallel$ to show a peak as is depicted in Figure 2.1b. This kind of behaviour has indeed been observed in several antiferromagnets such as Cr, α-Mn and some rare earth metals (Meaden, 1965).

We finally turn briefly to the case of a ferromagnet. The resistivity anomaly near the Curie temperature T_C was first explained by Fisher and Langer (Fisher and Langer, 1968) for $T > T_C$, and later was extended to the case of $T < T_C$ by Richard and Geldart (Richard and Geldart, 1973). The derivative of the resistivity near the ferromagnetic transition generally goes like the specific heat:

$$d\rho/dT \propto C(T) \propto t^{-\alpha} \qquad (2.26)$$

where $t=|T-T_C|/T_C$ is the reduced temperature, C(T) the specific heat and α the critical exponent of the specific heat. The experimental values of α for magnetic systems generaly lie in the range of -0.3 ~ 0.3 (Collins, 1989).

C Hall Effect In Magnetic Metals

2.6 The Ordinary Hall Effect

Consider a rod-shaped specimen with a electrical current J_x flowing along the x direction and a magnetic field B applied along the z direction, as depicted in Figure 2.4. Carriers moving along the x direction with charge q and velocity v will be subject to a Lorentz force qvB due to the presence of the magnetic field. Such a force will deflect electrons towards the -y direction. Since there is no current flowing along the y direction, a charge build-up must occur which in turn generates an electric field E_y to exactly balance the Lorentz force. That is:

$$E_y = qvB \tag{2.27}$$

Assuming that the electrons have an average velocity v, the current density can be expressed as:

$$J_x = qnv \tag{2.28}$$

where n is the density of carriers of charge q. Combining equation (2.19) and (2.20), we have:

$$E_y = J_xB/nq \tag{2.29}$$

The quantity defined by

$$R_H = E_y/J_xB = 1/nq \tag{2.30}$$

is called the **Hall coefficient** (Hurd, 1972). We note immediately that if electrons are the charge carriers, the Hall coefficient is negative: $R_H = -1/ne$ where e is the magnitude of the electron charge. The same result can be

obtained through a more formal and sophisticated analysis assuming an isotropic relaxation time τ.

2.7 The Anomalous Hall Effect

An anomalous behaviour often arises in the Hall effect of Kondo lattice compounds and magnetic metals in general. This anomalous Hall effect is much larger than the ordinary Hall effect in normal non-magnetic metals. The sign of this anomalous Hall effect is often positive, and the temperature dependence generally follows the magnetization of the system. One of the theoretical models to account for this anomalous Hall effect was first proposed by Smit (Smit, 1958) to account for the anomalous Hall effect in ferromagnets. The model was further developed for dilute magnetic systems (Fert, 1973).

The model is based on the idea of a skew scattering process by localized magnetic moments. Skew scattering occurs when the probability of scattering has a left-right asymmetry, i.e., the probabilities of scattering from $\mathbf{k}$ to $\mathbf{k}'$ and from $\mathbf{k}'$ to $\mathbf{k}$ are different. Such a process will favour the scattering one way (say to the left) over the other which in turn yields additional contribution to the Hall effect. More recently, Fert and Levy have extended this theoretical model to explain the anomalous Hall effect in Kondo lattice and heavy-fermion systems (Fert and Levy, 1987). We briefly follow the line of Fert and Levy. We begin by noting that the simplest form of the exchange interaction between the conduction electrons and

the localized f electrons is:

$$H_{exchange} = -J\mathbf{s}.\mathbf{j} + \lambda \mathbf{l}.\mathbf{j} \qquad (2.31)$$

where **s** and **l** are the spin and orbital angular momenta of the conduction electrons and **j** is the total angular momentum of the localized f electrons. The first term in (2.31) is real and symmetric. However, since the matrix element $\langle \mathbf{k}'|\mathbf{l}|\mathbf{k}\rangle = -\langle \mathbf{k}|\mathbf{l}|\mathbf{k}'\rangle$, the second term which contains **l** must be imaginary and antisymmetric (Fert and Hamzic, 1980). It is the presence of this **l.j** term in the hamiltonian that leads to the skew scattering, as we will see below.

Including the exchange hamiltonian of (2.31), the total hamiltonian can be generally written in the following form:

$$H = \sum_{k,k'} c^{+}_{k'} c_k (V_{kk'} + iW_{kk'}) \qquad (2.32)$$

where $V_{kk'}$ and $W_{kk'}$ are real with

$$V_{kk'} = V_{k'k}; \qquad W_{kk'} = -W_{k'k}.$$

Because of the presence of the antisymmetric term $W_{kk'} = -W_{k'k}$, the transition matrix to the third order contains antisymmetric terms of the following form:

$$-\left(\frac{2\pi}{\hbar}\right)\sum_{q} V_{kq} V_{qk'} W_{kk'} \delta(\epsilon_k - \epsilon_{k'}) \delta(\epsilon_k - \epsilon_q) \qquad (2.33)$$

It is the presence of these antisymmetric terms in the total transition matrix that leads to the skew scattering

probability. Using the skew scattering probability and the general expression of the Hall resistivity (defined as $\rho_H=R_HB$ where B is the magnetic field), Fert and Levy derived the following expression for the anomalous Hall coefficient:

$$R_H = C\mu_B k_B^{-1}\rho_m\chi \qquad (2.34)$$

where ρ_m is the resistivity of magnetic origin and C is a constant determined by the phase shifts during the scattering process:

$$C = -(5/7)g\sin\delta_2\cos\delta_2 \qquad T > T_K \qquad (2.35)$$

$$C = -\frac{5\pi}{21}g\frac{\sin(2\delta_3-\delta_2)\sin\delta_2}{\sin^2\delta_3} \qquad T < T_K \qquad (2.36)$$

where δ_i is the phase shift in the l=i channel (or in the partial wave with l=i) and g the Lande g-factor.

It should be emphasised here that, because of the dependence on the phase shifts, the constant C may not be all that "constant" in a real system as different magnetic phases may well have very different scattering potentials.

D Thermoelectric Power

2.8 Diffusion Thermoelectric Power

When a conductor is placed in a thermal gradient, the electrons at the hot end of the conductor will acquire more energy and will diffuse toward the cold end. Similarly, the electrons at the cold end will diffuse toward the hot end.

However, the diffusion rate is greater for the hot electrons due to the larger velocities and therefore, such a diffusion process will result in a net electron current. This current will cause a charge build-up at the cold end and thereby produce an electric field which opposes the further flow of electrons, reaching a steady state. If we write this electric field as E_d, then the diffusion thermoelectric power S_d can be defined through the relation of $E_d = S_d \nabla T$ where ∇T is the temperature gradient. For a metal, there is the following expression of S_d derived by solving the Boltzmann transport equations (Blatt et al, 1976):

$$S_d = \frac{\pi^2}{3} \frac{k^2 T}{e} \left(\frac{\delta \ln \sigma}{\delta \epsilon} \right)_{\epsilon_F} \qquad (2.37)$$

where σ is the conductivity and ϵ_F is the Fermi energy. For a simple metal, the logarithmic derivative of (2.37) takes the value of $3/\epsilon_F$ so the diffusion thermoelectric power is linear in temperature. Electron diffusion is only one of the mechanisms which give rise to thermal electricity, as we will see later. The phenomenon in general is called the Seebeck effect (Blatt et al, 1976).

2.9 Phonon and Magnon Drag Thermoelectric Power

As a result of the thermal gradient, a phonon current transporting the heat should be also present. An electron within the metal will be more likely to absorb a phonon

travelling from the hot end to the cold end. Therefore, the electron distribution will tend to absorb the phonon momentum in the $-\nabla T$ direction and will be "dragged" along by the phonon current as in viscous flow. Consequently, electrons tend to pile up at the cold end, generating a thermoelectric field in addition to the one we just discussed. The magnitude and temperature dependence of this phonon-drag thermopower, denoted as S_g, may be estimated as follows: Consider an acoustic wave propagating along the x direction through an isotropic medium containing sound-absorbing particles (electrons). The phonon pressure (similar to radiation pressure) is related to the decay of phonon energy by $p_x = -(dU/dx)$ (Blatt et al, 1976). In a steady state this force must be balanced by the opposing electric force $F_x = -n_o e E_x$ where n_o is the electron density. Replacing the energy density of phonons by the specific heat per unit volume C_g, one obtains $dU/dx \approx C_g(dT/dx)$. Hence we have:

$$E_x \approx (C_g/n_o e)(dT/dx) \tag{2.38}$$

and hence the corresponding thermopower:

$$S_g = C_g/n_o e \tag{2.39}$$

As the phonon specific heat is proportional to T^3 at low temperatures and T at high temperatures, we expect the phonon drag thermopower to follow the same temperature dependence:

$$S_p \propto T^3 \qquad T<<\theta_D \tag{2.40}$$

$$S_p \propto T \qquad T>>\theta_D \tag{2.41}$$

By the same token, magnon drag should also generate a corresponding contribution to the thermopower in a way

analogous to the phonon-drag thermopower. That is:

$$S_m \approx C_m/n_o e \qquad (2.42)$$

where C_m is the magnon specific heat. At low temperatures, C_m varies as $T^{3/2}$ for a ferromagnet (FM) and T^3 for an antiferromagnet (AF), we therefore expect the following behaviour for magnon-drag thermopower at low temperatures:

$$S_m \propto T^{3/2} \qquad \text{(FM)} \qquad (2.43)$$

$$S_m \propto T^3 \qquad \text{(AF)} \qquad (2.44)$$

E Specific Heat

2.10 Low-Temperature Specific Heat of Metals

The specific heat of a normal metal usually contains a contribution from free charge carriers which is linear in temperature and a contribution from phonons which rises as the cube of the temperature for temperatures well below the Debye temperature θ_D:

$$c_p(T) = \gamma T + \beta T^3 \qquad (2.45)$$

If c_p is the molar specific heat then γ value is given by (Grimvall, 1981)

$$\gamma = \frac{\pi^2 k_B^2 N_A\, m^*}{\hbar^2 (3\pi^2 n)^{2/3}} \qquad (2.46)$$

where N_A is the Avogadro's constant, n is the density of electrons and m^* is the effective mass of the electrons, and the β value is related to the Debye temperature θ_D:

$$\beta = 1941\theta_D^{-3} \qquad (2.47)$$

As a common practice, the specific heat data are often

analyzed by plotting c_p/T against T^2 to extrapolate γ and β which in turn gives the Debye temperature. The γ value is of importance since it can provide information about the effective mass of the conduction electrons. The linear temperature dependence of the electronic contribution to the specific heat comes about because only those electrons within k_BT of the Fermi energy can be thermally excited at temperature T; each of them has thermal energy $\sim k_BT$, so the total thermal energy of the electrons involved is proportional to T^2. The specific heat is defined as the temperature derivative of the thermal energy, hence the specific heat of this origin should be linear in T. For the phonon part of the specific heat, we expect a cubic term of T because the number of phonons thermally excited at temperature T is proportional to T^3, and each phonon has thermal energy of k_BT so the total thermal energy of phonons involved is proportional to T^4. For magnetic metals, contributions of magnetic origin will add additional terms to the expression of (2.45).

CHAPTER 3

EXPERIMENTAL TECHNIQUES

3.1 Electrical Transport Measurements

The station used for transport measurements consists of a helium cryostat placed in an electromagnet or a superconducting magnet, a sample probe with a vacuum jacket and a PC-computer controlled data acquisition system. A schematic diagram of the transport station with electromagnet is shown in Figure 3.1.

The water-cooled electromagnet is capable of producing a magnetic field up to 1.6 Tesla with stability for many hours. It can be either changed continuously or varied discretely. A coil positioned between the pole pieces of the magnet provides negative feedback for the current control unit to stabilize the field. A Rawson Rotating Gaussmeter is used to determine the field strength. The magnet can also be rotated by angles up to 360° which is essential for the Hall effect measurements.

The superconducting magnet is the solenoid type manufactured by Oxford Instruments, and is capable of producing axial magnetic field up to 8.5 Tesla. A stable HP-6260B DC power supply is used to energize the magnet. The

Figure 3.1

Block diagram of the Electrical Transport Measurement Station.

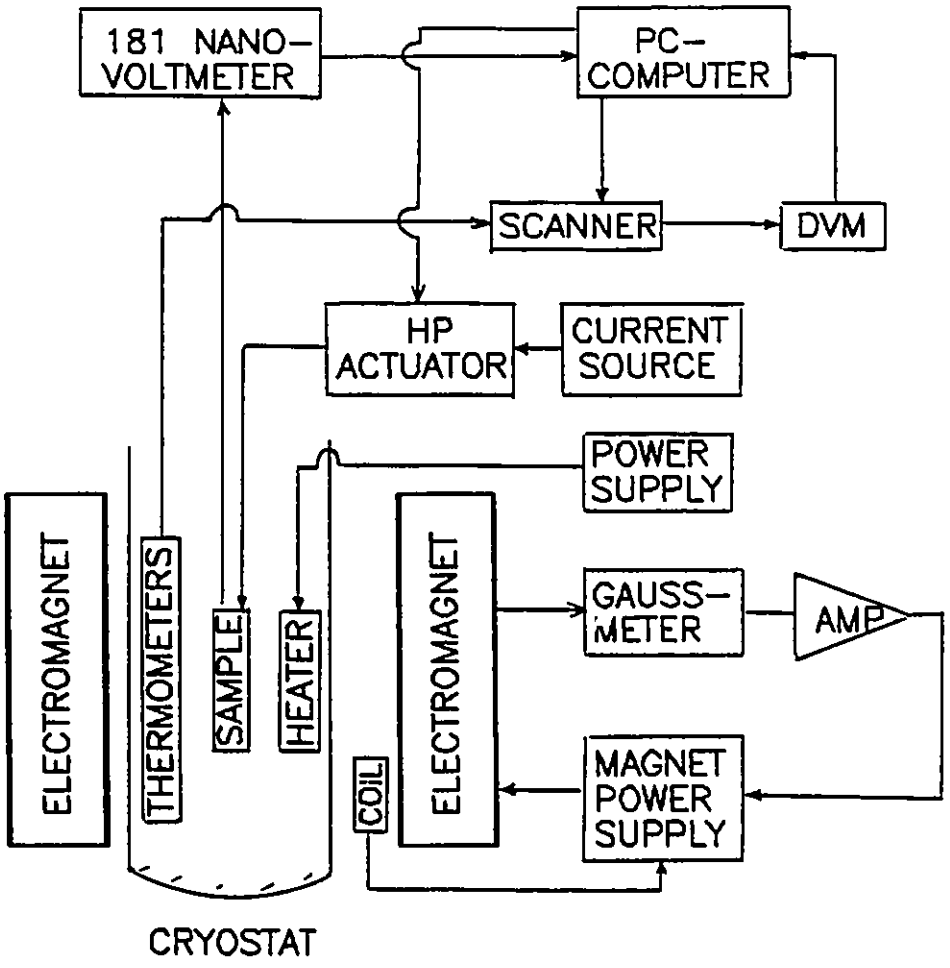
181 NANO–
VOLTMETER
PC–
COMPUTER
SCANNER
DVM
HP
ACTUATOR
CURRENT
SOURCE
POWER
SUPPLY
ELECTROMAGNET
THERMOMETERS
SAMPLE
HEATER
COIL
ELECTROMAGNET
GAUSS–
METER
AMP
MAGNET
POWER
SUPPLY
CRYOSTAT

field strength is determined through the pre-calibrated field/current ratio of 0.117 Tesla/Amps.

The sample probe used for the resistivity and Hall effect measurements consists of a brass top plate, a sample chamber with vacuum jacket (see Figure 3.2), two pumping lines and a helium transfer tube which also serves as the main support of the entire probe. At the bottom of the probe, the pumping lines terminate into two separated cavities: one is the sample chamber enclosed by a brass can while the other is a vacuum chamber enclosed by a stainless steel can, which surrounds the brass can. The sample chamber and the vacuum jacket are each sealed with six small screws and an indium O-ring. The vacuum jacket (the space in between the cans) can be pumped to provide a vacuum space. Such a vacuum space is essential to isolate the sample chamber from the surrounding liquid helium and to allow a better control of the temperature. Inside the chamber, there is a plate-like brass sample holder which is thermally isolated from the rest of the probe by a piece of kel-F rod. The sample is placed on the flat face of the brass plate while the thermometers are buried inside the plate. Such a configuration provides excellent thermal contact between the thermometers and the sample. The temperature is varied by a heater wound on the outside of the inner can, and is monitored by calibrated carbon glass and platinum resistor thermometers. The sample chamber is normally pressured with 5 to 10 psi (gauge) helium gas to

Figure 3.2

Schematic diagram of the probe for transport measurements.

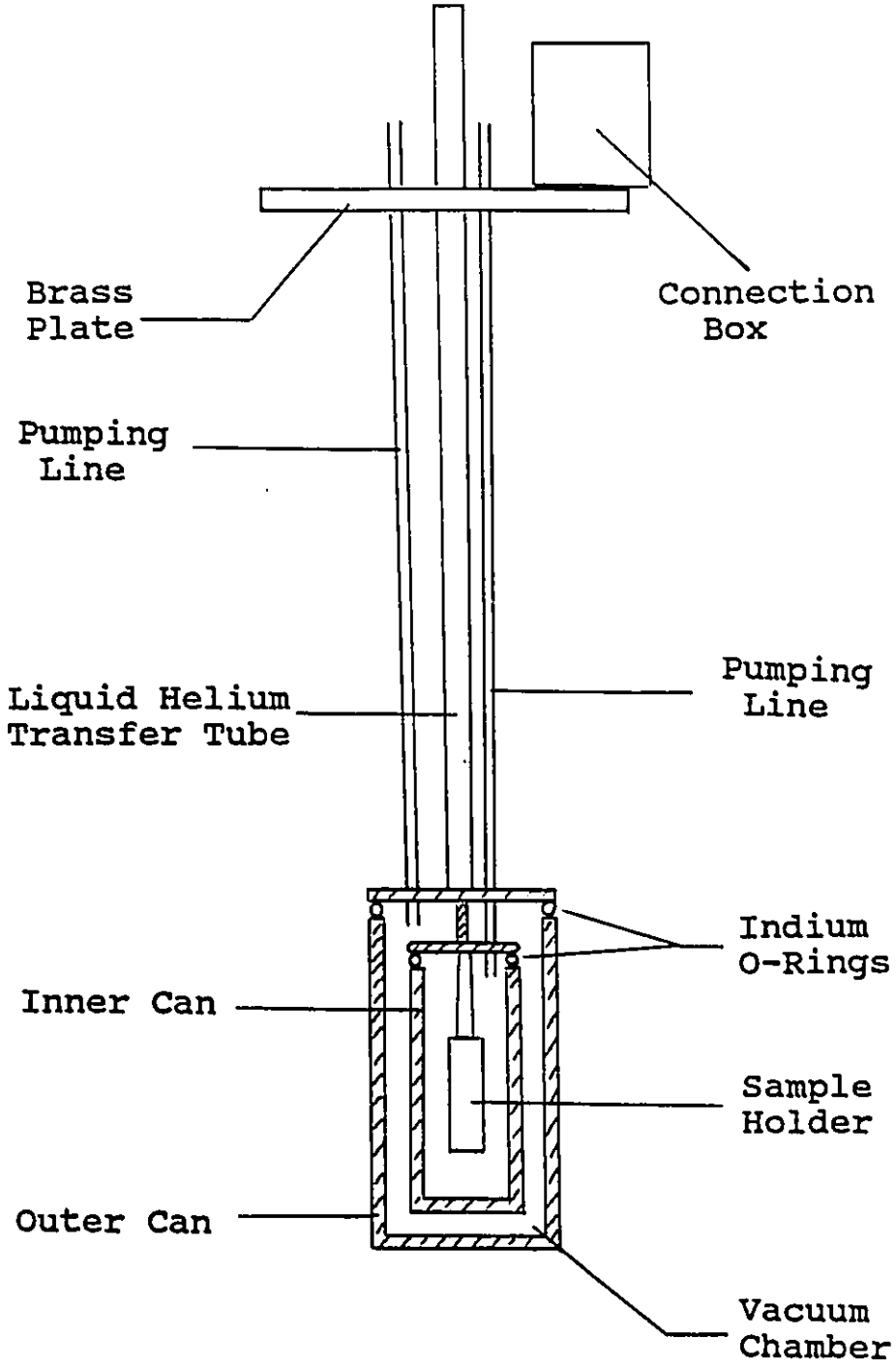
Brass Plate
Connection Box
Pumping Line
Liquid Helium Transfer Tube
Pumping Line
Indium O-Rings
Inner Can
Sample Holder
Outer Can
Vacuum Chamber

ensure uniform heating. The wires for electrical connections are extended out of the chamber through a thin stainless steel tube with both ends sealed with epoxy. Similarly, the wires pass through the top plate in a sealed tube and are finally joined to the connection box mounted on the top plate. All the wires from the sample chamber run continuously to the connection box to minimize stray and thermal voltage. The two pumping lines are regulated by two valves also mounted on the top plate. Each valve is connected to a copper pipe which can be connected to either a vacuum pump or a helium gas cylinder.

The probe used for thermopower measurements is very similar to the one described above, except that the sample holder inside the chamber this time is made of kel-F, a reasonable thermal insulator which allows the establishing of a temperature gradient with ease.

The helium cryostat consists of a cryogenics Dewar with evacuated vacuum jackets and a sleeve for liquid nitrogen. The inner chamber is sealed with a rubber O-ring to the bottom of the probe's brass top plate, at the top of the cryostat. An outlet regulated with valves is provided for gaseous helium which boils off during the experiment.

The wires from the connection box mounted on the top of the brass plate of the probe are connected to the central connection box mounted close to the PC computer station through well shielded cables. They are finally jointed to either the HP-59306A Relay Actuator (for current reversal), DC

current source, the Keithley Model 705 Scanner, or the Keithley 181 nanovoltmeter.

DC current for the transport measurements and thermometers is supplied by two independent battery driven current sources which can be adjusted in the range of 0.1μA-100mA. For resistivity measurement, the current direction is switched after each measurement using the HP Relay Actuator and the sample voltage is monitored by the Keithley 181 nanovoltmeter. The polarity reversal and the subsequent averaging procedure are needed to eliminate the offset voltage and other spurious signals.

The resistivity of the samples is measured with the conventional four-probe method: two for applying the DC current and two for measuring the voltage. The samples used are typically of the dimensions of 5x1.5x0.2mm^3, and all the electrical contacts are made of silver paste with a typical contact resistance of 2~3 Ω. The current values used are typically in the range of 5-20 mA. As mentioned above, reversal of the current direction was carried out to eliminate spurious effects.

The Hall voltage is also measured in the four-probe configuration with two for the DC current and two for the Hall voltage. The standard procedure for Hall voltage measurement is as follows: at a given temperature, a voltage reading is taken first with the field applied perpendicular to the flat face of the sample, then a second voltage is taken after

reversing the magnetic field. The Hall voltage is calculated as:

$$V_H = 1/2[V(H)-V(-H)] \qquad (3.1)$$

Such a procedure is necessary to eliminate the offset signal resulting from the mismatch of the two Hall contacts.

The thermoelectric power (or thermopower for short) was measured by a differential method, that is, a small temperature gradient across the sample (ΔT) was generated and the corresponding thermal voltage (ΔV) was measured. The reference used was high purity thick lead wire which has well defined absolute thermopower. The thick lead wires were first slightly flattened, then mechanically pressed against the two ends of the sample with plastic screws to form the electrical contacts (junctions). A small heater was placed under one of the lead-sample junctions. The thermometers were embedded in small brass blocks which were then thermally attached to the flat lead wires at each of the two junctions. The other two ends of the lead wires were brought to and thermally attached onto a brass block far away from the sample. Two thin copper wires were then electrically joined to the two ends of the lead wires on this brass block and run through the top plate of the probe for thermal voltage measurements. The measured signal contains both the thermal voltage of the lead and that of the sample, that is to say: if T is the temperature at the cold end of the sample and $T+\Delta T$ the temperature at the hot end, then the voltage of the sample is $-S\Delta T$ while that of the

lead wire is $S_p\Delta T$, assuming that S is the thermopower of the sample and S_p the one of Pb. The total voltage measured is then:

$$\Delta V = (S_p - S)\Delta T \qquad (3.2)$$

From this expression, one can easily calculate the thermopower of the sample:

$$S = S_p - \Delta V/\Delta T \qquad (3.3)$$

3.2 DC Susceptibility Measurements

The susceptibility is measured with a Quantum Design SQUID magnetometer. A schematic block diagram of the SQUID magnetometer is shown in Figure 3.3. The sample is mounted on a travelling rod in a cryostat. A superconducting magnet generates fields up to 5 Tesla along the direction of the rod, referred to as the axial direction. The temperature of the inner chamber is stabilized through a helium exchange gas. Three superconducting coils, wound about the rod in the axial direction are connected together. The central coil is counter-wound with respect to the coils above and below and has twice as many turns. At a given temperature, a stepping motor controlling the axial motion (up and down) of the sample rod is activated. The axial magnetic field generated by the superconducting magnet creates an axial magnetic moment in the sample. Each single axial step of the sample induces a current pulse in the coils according to the position of the sample in the coil configuration. The signal is inductively coupled to a SQUID and accurately measured. A complete trip of the sample

Figure 3.3

Block diagram of the SQUID magnetometer used for the magnetic susceptibility measurements.

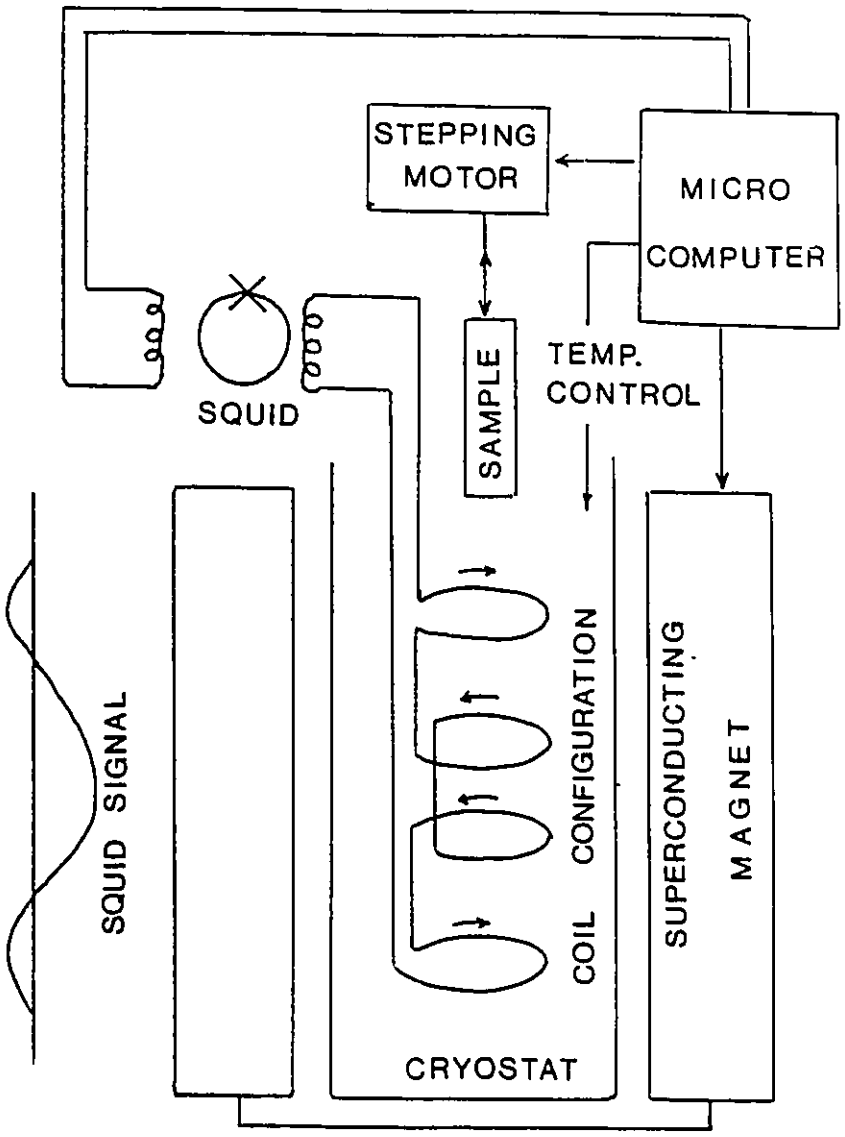
STEPPING MOTOR
MICRO COMPUTER
SQUID
SAMPLE
TEMP. CONTROL
SQUID SIGNAL
COIL CONFIGURATION
SUPERCONDUCTING MAGNET
CRYOSTAT

through the coil configuration will generate a graph of signal versus sample position. The normalized square root of the sum of squares of these data points is proportional to the magnetization of the sample.

The entire unit is highly automatic, the controls of temperature, field, the motion of sample and data acquisition are all done automatically by a microcomputer based control unit. The system is periodically calibrated with a standard palladium sample to ensure the accuracy of absolute measurements.

3.3 Specific Heat Measurements

The specific heat was measured by A. Le Dawson of McGill university by a conventional thermal relaxation method with an apparatus similar to the one described by Bachmann et al. (Bachmann et al, 1972). A block diagram of the apparatus is shown in Figure 3.4. In the set-up, the sample is thermally attached onto one face of a small sapphire slide which serves as a sample holder. On the other side of the slide, there is a thin layer of evaporated constantan film (~1kΩ) which was cut into two halves with one of them serving as a heater. On the other half, an Au+0.07%Fe--Chromel thermocouple was attached with silver epoxy which measures the temperature of the sample. The sample and the addenda (everything else including the sample holder, heater, thermocouple and epoxies) were then thermally linked to a large copper block through the

Figure 3.4

Block diagram of the specific heat measurement apparatus.

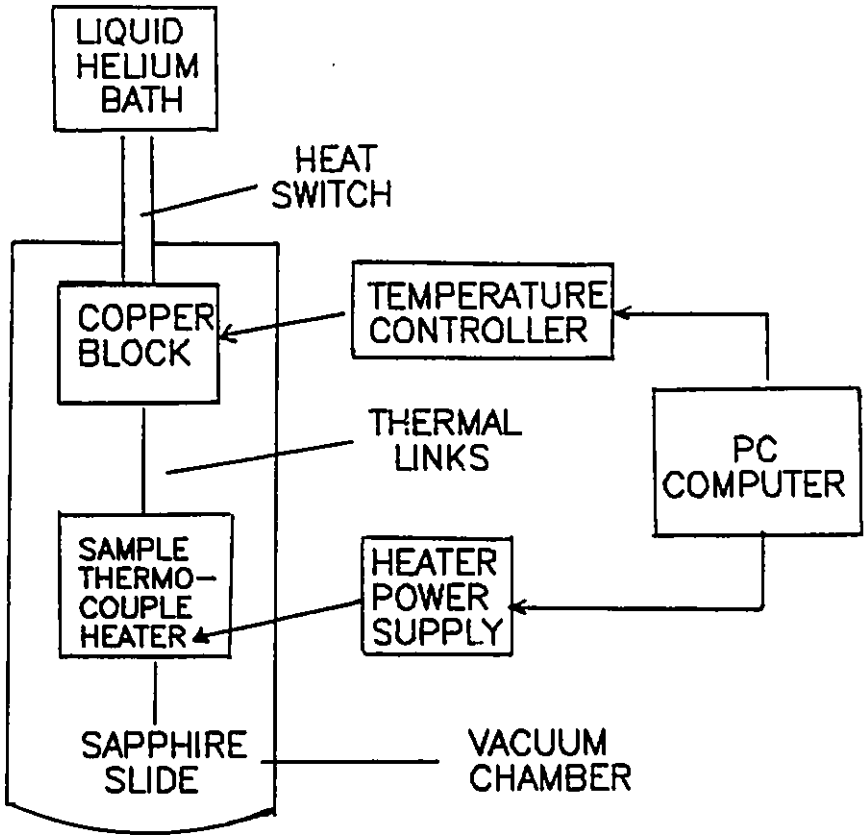
LIQUID HELIUM BATH
HEAT SWITCH
COPPER BLOCK
TEMPERATURE CONTROLLER
THERMAL LINKS
PC COMPUTER
SAMPLE THERMO-COUPLE HEATER
HEATER POWER SUPPLY
SAPPHIRE SLIDE
VACUUM CHAMBER

thermocouple wires and the current leads of the heater (constantan film). The copper block serves as a heat reservoir on which the reference junction of the Au+0.07%Fe--Chromel thermocouple was also attached (see Figure 3.4 for more details).

The basic principles involved are outlined as follows: Suppose that the heat reservoir (copper block) is stabilized at a temperature T_o, and the sample and the addenda are at a temperature $T=T_o+\Delta T$ with the heater power on. The total specific heat of the sample and the addenda is simply $C = dQ/dT$ which can also be written as:

$$C = \frac{dQ/dt}{dT/dt} \tag{3.4}$$

where dQ/dt and dT/dt are the time-derivatives of the heat transfer and temperature. For small ΔT, the power leaking out of the sample and the addenda through all the links can be approximated as $K(T_o)\Delta T$ where $K(T_o)$ is the thermal conductivity of all the thermal links at temperature T_o. The time-derivative of Q is then given by:

$$dQ/dt = P - K(T_o)\Delta T \tag{3.5}$$

where P is the power of the heater. If the power of the heater is turned off suddenly at time t=0, then from (3.5), one obtains $dQ/dt=-K\Delta T$. Noting that $dT/dt=d\Delta T/dt$, one finally arrives at the following expression for the total specific heat C:

$$C = \frac{-K(T_o)\,\Delta T}{d\Delta T/dt} \tag{3.6}$$

Assuming the value of C is constant over the temperature range ΔT, one finally has:

$$\Delta T(t) = \Delta T(0)\exp(-t/\tau) \tag{3.8}$$

$$C = K(T_o)\,\tau \tag{3.9}$$

Thus measuring K and τ constitutes a measurement of C.

The relaxation time τ can be measured by measuring $\Delta T(t)$ as a fuction of time, and the value of K of a given material (say copper) is known. To actually get the specific heat of the sample, a calibrating run without the sample is needed to determine the specific heat of the addenda which is later subtracted from the total specific heat C to get the sample specific heat.

CHAPTER 4

UNi_2Si_2

4.1 Introduction

UNi_2Si_2 crystallizes in the $ThCr_2Si_2$ type of crystal structure mentioned in Chapter 1 and has been studied previously by neutron diffraction and magnetization measurements. Neutron-diffraction studies by Chelmicki et al. (Chelmicki et al, 1985) showed that UNi_2Si_2 undergoes a magnetic phase transition at T_N=103 K to a collinear antiferromagnetically ordered state (AF1). At 53 K, the system undergoes a second phase transition into a commensurate longitudinal spin density wave (LSDW) state. The magnetic moments in this system are associated with the uranium atoms and are aligned along the c axis in the ordered states. In contrast, magnetization studies (Chelmicki et al, 1985; McElfresh et al, 1990) showed ferromagnetic ordering below 98 K and no evidence of a phase transition at 53 K. More recently, neutron diffraction studies of single crystal samples by Lin et al. (Lin et al, 1991) confirmed the presence of the two magnetically ordered phases and, in addition, established a third magnetically ordered phase, between 103 K and 123 K, which is an incommensurate longitudinal spin density wave state. The studies also revealed that the

longitudinal spin density wave state below 53 K is accompanied by a net ferromagnetic moment of 1.0 ± 0.3 μ_B per U-atom along the c axis. The commensurate LSDW state has a periodicity of 3c and the incommensurate one has a periodicity slightly smaller than 4c, where c is the lattice parameter of the tetragonal c axis (Lin et al, 1991).

4.2 Sample Preparation

The single crystal of UNi_2Si_2 used in this study was prepared from U, Ni, and Si ingots which were premelted, cleaned where applicable, and weighed. They were reacted and homogenized in an inert gas atmosphere in an arc furnace with a water-cooled hearth. The single crystal was grown by the Czochalski technique in a Reed-type triarc furnace which had been modified to include a water-cooled hearth and a seed rod. Argon gettered with titanium was used at 100 kPa as the chamber atmosphere. The samples for various measurements were cut parallel and perpendicular to the tetragonal c axis with a spark cutter. X-ray measurements established that the samples were single crystals with lattice parameters a=3.96 Å and c=9.51 Å.

4.3 Magnetic Susceptibility

The magnetic susceptibility (M/H) has been measured in a magnetic field of 1.6 Tesla with the fields applied parallel ($\chi_{/}$) and perpendicular ($\chi_{\perp}$) to the c axis. The result is shown

in Figure 4.1. The susceptibility is very anisotropic, with $\chi_{/\!/}$ exceeding $\chi_{\perp}$ by a factor of 3 at room temperature and 54 at 5 K.

From room temperature down to about 130 K, the susceptibility obeys the Curie-Weiss law, as can be seen from the temperature dependence of the inverse susceptibility shown in Figure 4.2. A best fit for temperatures above 130 K with the expression

$$\chi = C/(T-\theta_{CW}) \qquad (4.1)$$

yields θ_{CW} =-530 K and μ_{eff}=3.55 μ_B for $\chi_{\perp}$, θ_{CW}=-15 K and μ_{eff}=3.67 μ_B for $\chi_{/\!/}$. The Curie-Weiss temperature θ_{CW} is very anisotropic indicating a strong confinement of moments along the c axis. The susceptibility starts to deviate from the Curie-Weiss behaviour at about 130 K where the system is about to enter a magnetically ordered phase (incommensurate LSDW) which sets in at 123 K. However, no sharp feature is observed in the vicinity of the 123 K transition.

At the Néel temperature T_N=103 K, a sharp peak characteristic of an antiferromagnetic transition is observed in $\chi_{/\!/}$. A similar feature is also present in $\chi_{\perp}$ but the magnitude is much too small to be seen on the scale of Figure 4.1.

As the temperature is further lowered, the onset of ferromagnetism occurs at about 78 K for H$\|$c. The ferromagnetism co-exists with the commensurate LSDW state (Lin et al. 1991); the transition temperature of this magnetic

Figure 4.1

Temperature dependence of the magnetic susceptibility of UNi_2Si_2 measured in a field of 1.6 Tesla. ▲: H∥c; □: H⊥c.

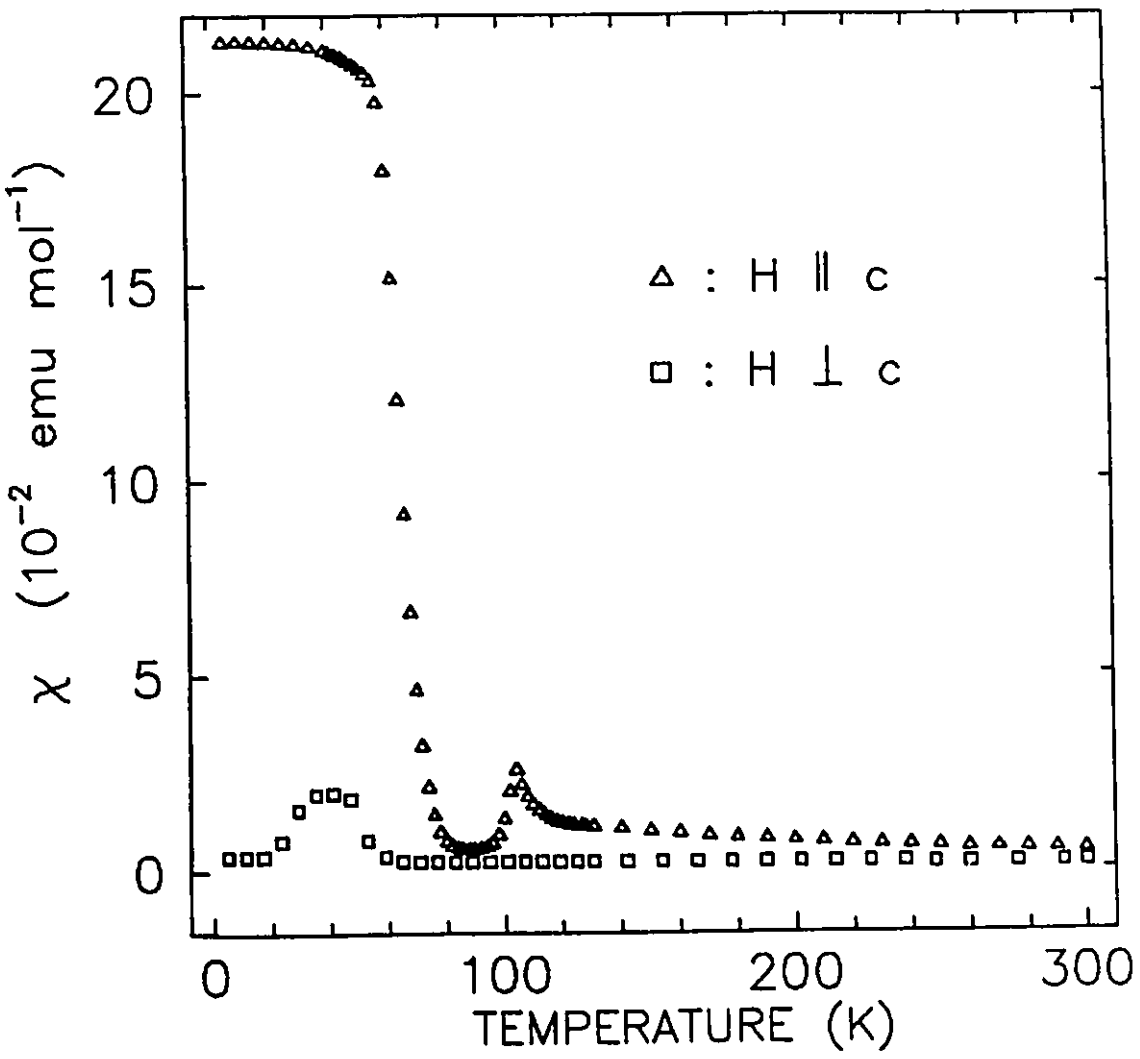
20
15
10
5
0
χ (10⁻² emu mol⁻¹)
△ : H ∥ c
□ : H ⊥ c
0
100
200
300
TEMPERATURE (K)

Figure 4.2

Temperature dependence of the inverse susceptibility of UNi_2Si_2 measured in a field of 1.6 Tesla. ▲: $H \| c$; □: $H \perp c$.

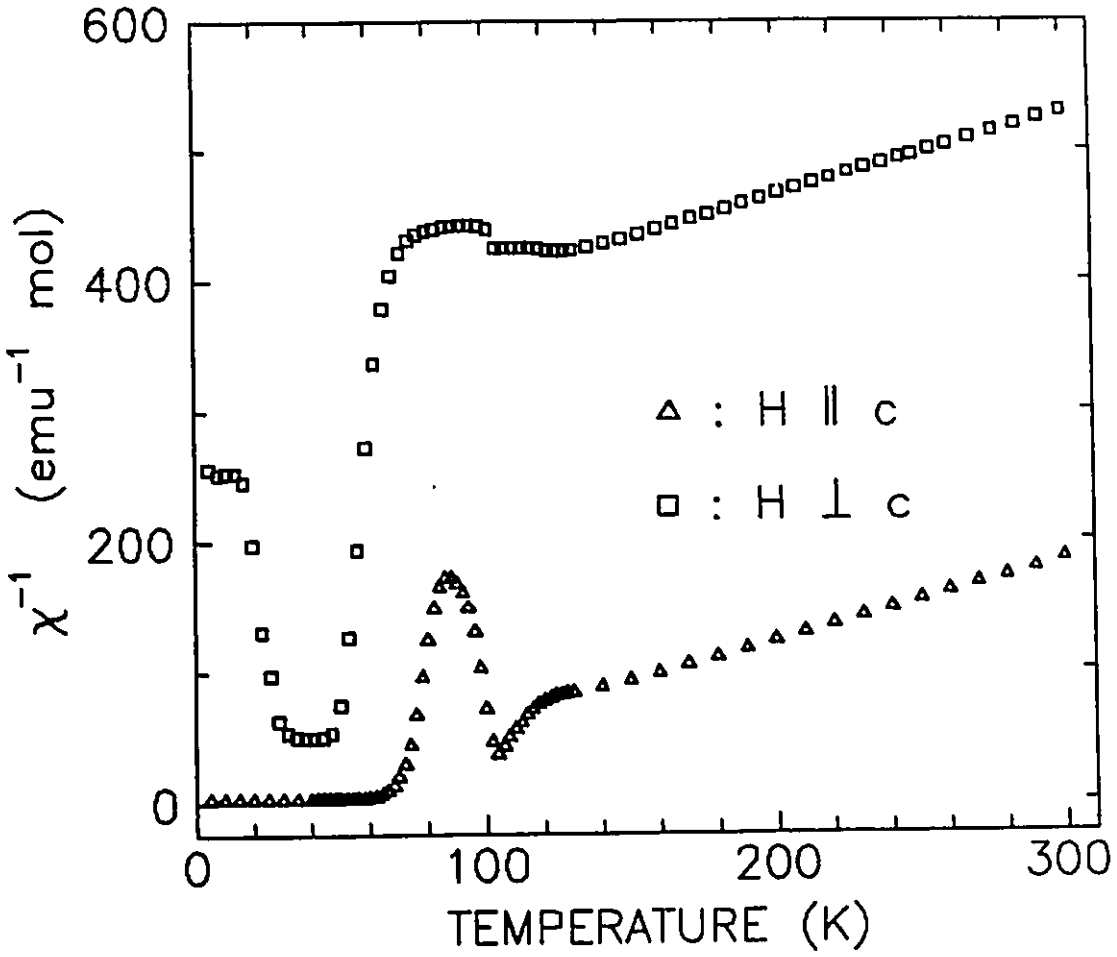
600
400
200
0
χ^{-1} (emu^{-1} mol)
△ : H ∥ c
□ : H ⊥ c
0
100
200
300
TEMPERATURE (K)

phase observed by neutron scattering is 53 K. The apparent increase of the transition temperature here is due to the 1.6 Tesla magnetic field applied along the c axis. Detailed discussion of the field dependence of this transition temperature will be postponed to section 4.5 of this chapter. The estimated ferromagnetic moment per uranium atom at 5 K with H=1.6 Tesla is 0.62 μ_B which is in reasonable agreement with the neutron diffraction result (Lin et al. 1991) of 1.0 ± 0.3 μ_B. The susceptibility perpendicular to the c axis ($\chi_\perp$), however, shows very different behaviour. It starts to increase at about 57 K and reaches a maximum of 2.0×10^{-2} (emu mol^{-1}) at about 40 K. Below 20 K, the susceptibility $\chi_\perp$ drops down to 3.9×10^{-3} (emu mol^{-1}) and remains at this value at low temperatures.

4.4 Electrical Resistivity

The dc resistivity of UNi_2Si_2, both parallel ($\rho_\parallel$) and perpendicular ($\rho_\perp$) to the tetragonal c axis, has been measured from 4.2 K to 300 K. The result is shown in Figure 4.3. The resistivity is very anisotropic. The room-temperature value of the resistivity is 226 $\mu\Omega$ cm for $\rho_\parallel$ and is 156 $\mu\Omega$ cm for $\rho_\perp$. At 4.2 K, the c-axis resistivity $\rho_\parallel$ decreases to 69 $\mu\Omega$ cm and the value of $\rho_\perp$ drops to 20 $\mu\Omega$ cm. The temperature coefficient $d\rho/dT$ is positive at all temperatures for $\rho_\perp$ but is negative for $\rho_\parallel$ down to 150 K. There are several distinct features that are associated with the three magnetic phase transitions: As

Figure 4.3

Temperature dependence of the resistivity of UNi_2Si_2 with the current parallel and perpendicular to the c axis. The dotted line was taken with decreasing temperature to show the thermal hysteresis.

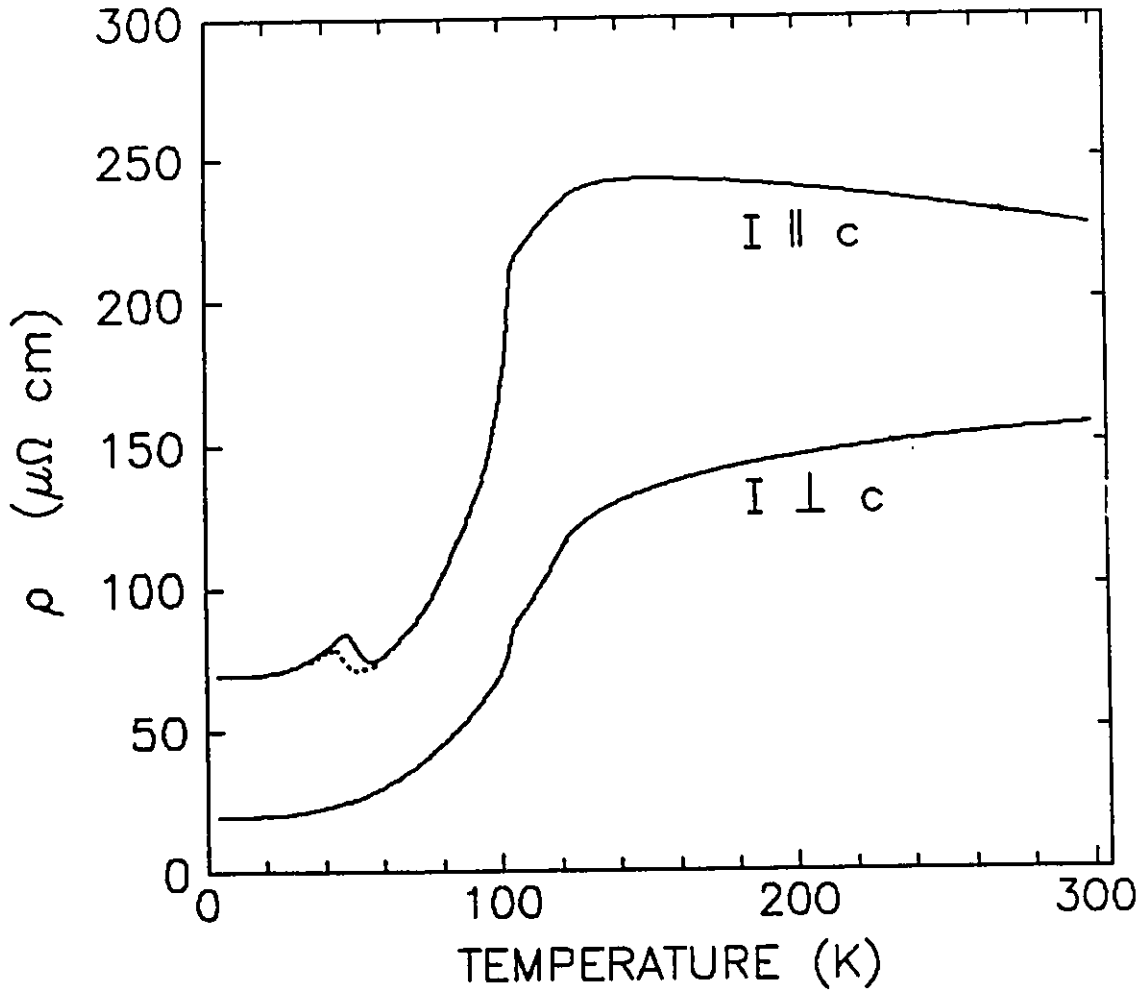
300
250
200
150
100
50
0
ρ (μΩ cm)
I ∥ c
I ⊥ c
0
100
200
300
TEMPERATURE (K)

the temperature is lowered, a drastic decrease in the resistivity along both directions occurs at about 123 K. A second feature occurs at about 103 K where the slope of $\rho_{/\!/}$ becomes much steeper while the resistivity perpendicular to the c axis $\rho_{\perp}$ develops a knee. As the temperature is lowered further, a local maximum occurs in $\rho_{/\!/}$ between 56 and 35 K, while the resistivity $\rho_{\perp}$ is very smooth in the same temperature range. The local maximum in $\rho_{/\!/}$ shows a temperature hysteresis of 4.5 K, as shown Figure 4.3.

The temperature dependence of the resistivity above 123 K is comparatively weak. Such a behaviour indicates that electron-phonon scattering does not dominate the contributions to the resistivity in this system and scattering of magnetic origins is more important. If we take the linear variation of $\rho_{\perp}$ above 200 K as coming from phonon scattering, then at room temperature the phonon contribution only makes up about 14% of the total resistivity $\rho_{\perp}$. The resistivity $\rho_{/\!/}$ at temperatures above 150 K has a negative slope and appears to be characteristic of the Kondo behaviour. A best fit with the expression

$$\rho = \rho_o + AT - B\ln T \qquad (4.2)$$

however, requires a negative value of A which is unphysical as it implies a negative phonon contribution to the resistivity. Such a result indicates that the resistivity in this temperature range is in a broad cross-over region from a Kondo behaviour at high temperatures to a non-Kondo behaviour

region, and one would need to extend the measurement to much higher temperatures to have a meaningful fit.

The resistivity at low temperatures is best described by a gapped spin wave term (Andersen et al, 1979) plus a T^2 term:

$$\rho = \rho_o + AT^2 + BT(1+2T/\Delta)\exp(-\Delta/T) \qquad (4.3)$$

where ρ_o is the residual resistivity, Δ the energy gap in the spin wave (magnon) spectrum, and A and B are constants. The best fit of the resistivity with this model is shown in Figure 4.4 for the temperature range of 4.2-45 K. The best-fit parameters are summarized in Table 4.1. Because of the large magnetic anisotropy in the system, as has been demonstrated by the magnetic susceptibility (section 4.3) and the neutron diffraction measurements (Lin et al, 1991), it is almost certain that an energy gap should be present in the spin-wave excitation (magnon) spectrum (Collins, 1991). Therefore it is not surprising that the gapped spin wave model works as well as it does. Note that the gap values Δ are rather comparable with those of URu_2Si_2 (Palstra et al, 1986; Dawson et al, 1989) obtained through the same procedure. The T^2 term is needed to have a good fit, particularly at the lowest temperatures (T<10 K) where the resistivity is best approximated by a T^2 temperature dependence. Palstra et al. and Dawson et al. also found it necessary to include a T^2 term in order to better fit the resistivity of URu_2Si_2 at low temperatures. These authors have attributed this T^2 term to a Fermi liquid behaviour

Figure 4.4

Resistivity of UNi_2Si_2 in the temperature range of 4.2-45 K. (a) $I \| c$; (b) $I \perp c$. The solid line is the best fit using the expression of $\rho = \rho_o + AT^2 + BT(1+2T/\Delta)\exp(-\Delta/T)$. The best-fit parameters are listed in Table 4.1. Some data points were omitted for clarity.

(a)

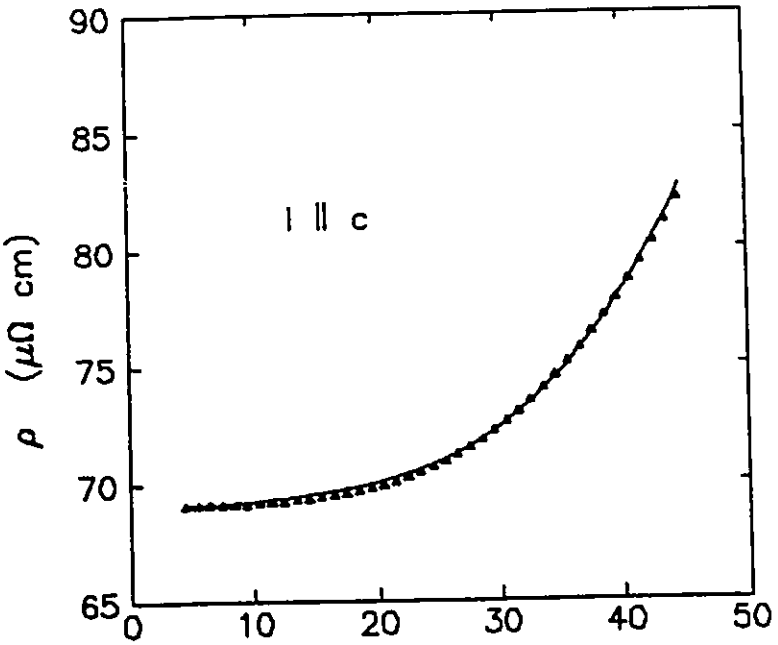
90
85
80
75
70
65
ρ (μΩ cm)
I ∥ c
0
10
20
30
40
50

(b)

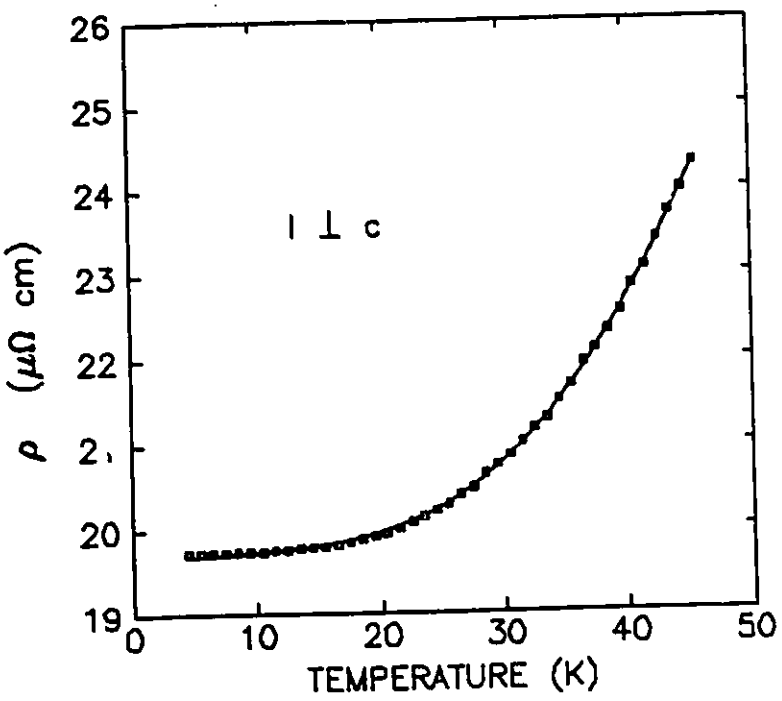
26
25
24
23
22
2
20
19
ρ (μΩ cm)
I ⊥ c
0
10
20
30
40
50
TEMPERATURE (K)

	Temp. Range	ρ_o ($\mu\Omega$ cm)	A ($\mu\Omega$ cm K^{-2})	B ($\mu\Omega$ cm K^{-1})	Δ (K)
I$\parallel$c	4.2-45K	70.03	1.16×10^{-3}	1.034	100.4
I$\perp$c	4.2-45K	19.67	5.89×10^{-4}	0.375	102.1

Table 4.1. Best-fit parameters obtained from fitting the low temperature resistivity of UNi_2Si_2 with the expression of $\rho = \rho_o + AT^2 + BT(1+2T/\Delta)\exp(-\Delta/T)$.

(Pines and Nozieres, 1966). Unfortunately, Fermi liquid behaviour is not the only one which gives rise to a T^2 dependence of the resistivity, and further more, both the theoretical prediction (Ashcroft and Mermin, 1976; Dugdale, 1977) and most of the reported experimental evidence (for reviews, see Steward, 1984; Coles, 1987; Ott, 1987) seem to suggest that the T^2 dependence should only be seen in very pure samples at extremely low temperatures (below 1K), although a higher upper bound (15 K) has been reported recently (Thompson et al, 1987). Therefore, it is still unclear up to what upper temperature the Fermi liquid behaviour holds and if it is indeed the mechanism behind the T^2 term so often observed in these heavy fermion compounds and Kondo lattice systems above liquid helium temperatures.

The strongest anisotropy of the resistivity comes from the behaviour in the vicinity of the 53 K phase transition where, a local maximum is seen in $\rho_{/\!/}$ while $\rho_{\perp}$ remains very smooth. This type of resistivity anomaly at the magnetic phase transition has been observed in several systems including Cr, α-Mn, Dy (Meaden, 1965) and URu_2Si_2 (Palstra et al, 1986; Dawson et al, 1989). In all the cases, the origin of the anomalous increase has been attributed to gapping of the Fermi surface by the formation of the magnetic Brillouin zone, as has been discussed in section 2.5 of Chapter 2. Because of the drastic change of the magnetic periodicity along the c axis at T_c=53 K, gapping of the Fermi surface may well be the case in

UNi_2Si_2. However, the situation here is somewhat different; the phase transition at 53 K is of first order (Lin et al, 1991), as is also indicated by the thermal hysteresis, and the term due to critical scattering should be absent in the model discussed in section 2.5 of Chapter 2. Furthermore, one can no longer use the critical approach to handle the temperature dependence of the energy gap Δ (which in turn gives rise to the T-dependence of the gap resistivity). In fact, for a first order phase transition, the energy gap should be a step function of temperature and goes from zero above T_c to a finite value Δ below T_c. In a real system, such a step function may be broadened, as in the case of UNi_2Si_2 (Lin et al, 1991). Despite all these differences, the anomalous increase of the resistivity ρ_f in the vicinity of 53 K can still be qualitatively explained by a broadened step function of the energy gap, as is depicted in Figure 4.5. Such a description is also consistent with the Hall effect result which will be discussed later in section 4.7.

4.5 Field Dependence of The Phase Transition Temperatures

In order to shed new light on the nature of these phase transitions, resistivity measurements under magnetic fields have been carried out. It is found that the two lower phase transition temperatures can change significantly when a magnetic field is applied **along the c axis.** No such change of the 123 K phase transition is seen within the experimental

Figure 4.5

Schematic diagram showing how the combined contribution of the resistivity from magnon scattering and gapping of the Fermi surface can generate the anomaly seen in ρ_f. Note that ρ^{Gap} has been shifted upward by an amount of $\rho(T_c)$ for clarity.

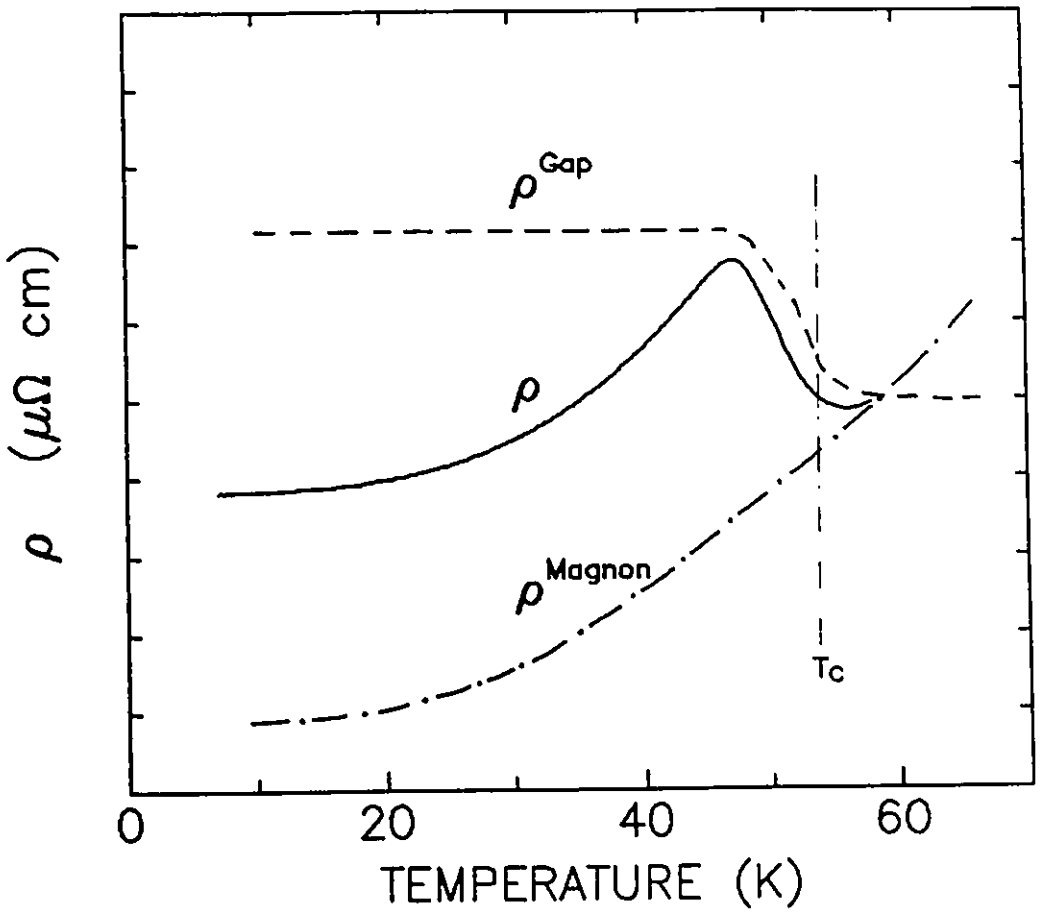
ρ (μΩ cm)
ρ Gap
ρ
ρ Magnon
Tc
0
20
40
60
TEMPERATURE (K)

uncertainty (~ 2 K in a field of 3.5 Tesla). In Figure 4.6, the resistivity $\rho_{/\!/}$ taken at 0 and 2.5 Tesla for a limited temperature range is plotted. One can note immediately that the anomaly associated with the 53 K transition in zero field moves up by 20 K in temperature in a 2.5 Tesla field. One also notices that the feature at 103 K in zero field moves down to lower temperature in an applied field. In contrast, the feature at 123 K remains virtually unchanged. A quantitative and also more sensitive way of describing these changes is to identify the features of the phase transitions in the temperature derivative of the resistivity $d\rho_{/\!/}/dT$. The low temperature phase transition is identified as the negative minimum in $d\rho_{/\!/}/dT$, the antiferromagnetic transition is identified as the peak in $d\rho_{/\!/}/dT$, and the 123 K transition is identified as the shoulder in $d\rho_{/\!/}/dT$, as indicated by the three arrows in Figure 4.7. In doing so, a temperature-field phase diagram is mapped out and is shown in Figure 4.8. The highest field at which the two low temperature phase transitions can still be identified is 3.5 Tesla. At still higher field, these two features are all washed out. Similar changes in the transition temperatures with magnetic field have also been observed independently by Lin et al. (Lin et al, 1990) with neutron scattering measurements up to 3 Tesla. In addition, they were able to identify a splitting of the 103 K phase above 2.5 Tesla, as shown by the dashed line in Figure 4.8.

Figure 4.6

Resistivity of UNi_2Si_2 measured with $I \| c$ in a magnetic field applied along the c axis. Solid line: H=0 Tesla; Dotted line: H=2.5 Tesla.

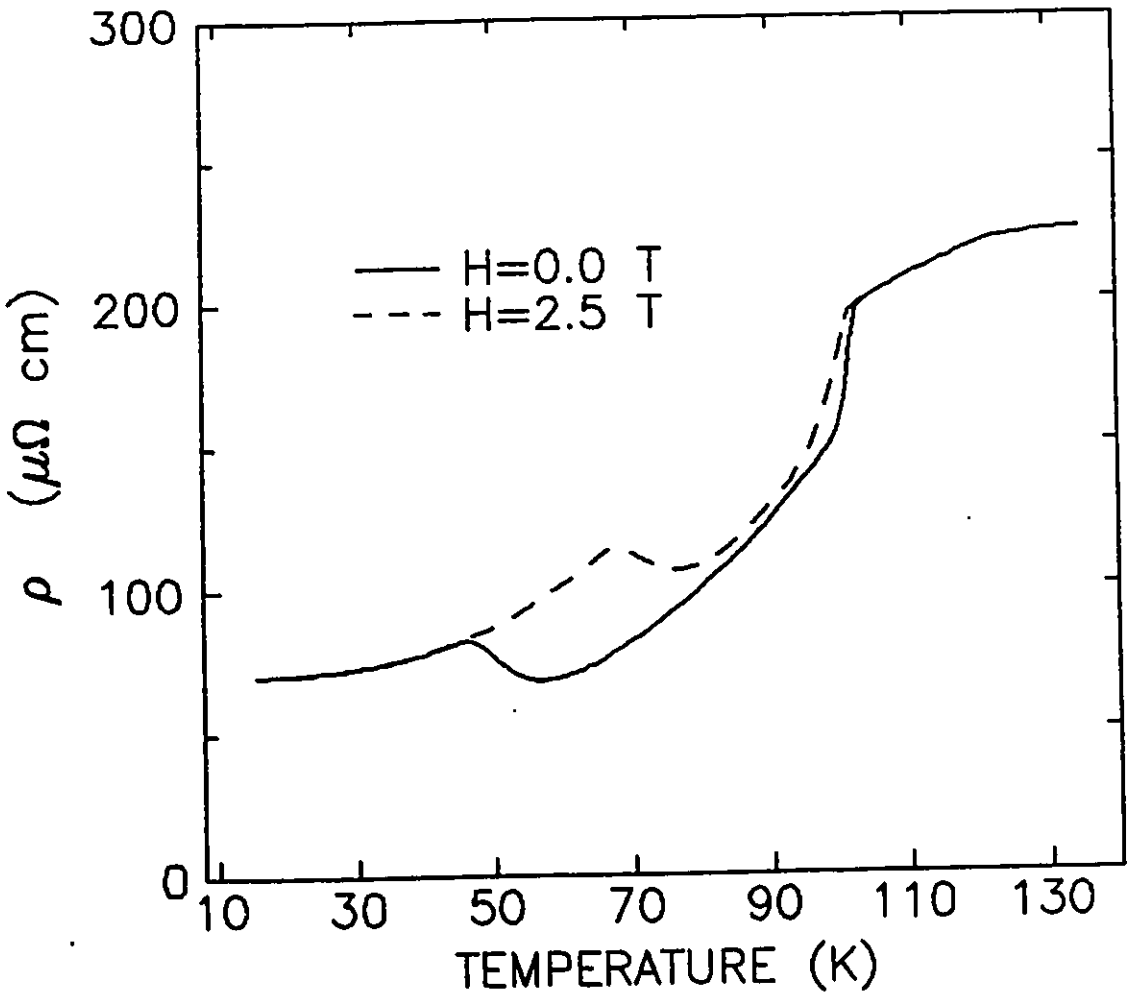
300
200
100
0
ρ (μΩ cm)
H=0.0 T
H=2.5 T
10
30
50
70
90
110
130
TEMPERATURE (K)

Figure 4.7

Derivative of resistivity of UNi_2Si_2 measured in a magnetic field. $I \| c$; $H \| c$. Solid line: H=0 Tesla; Dotted line: H=2.5 Tesla.

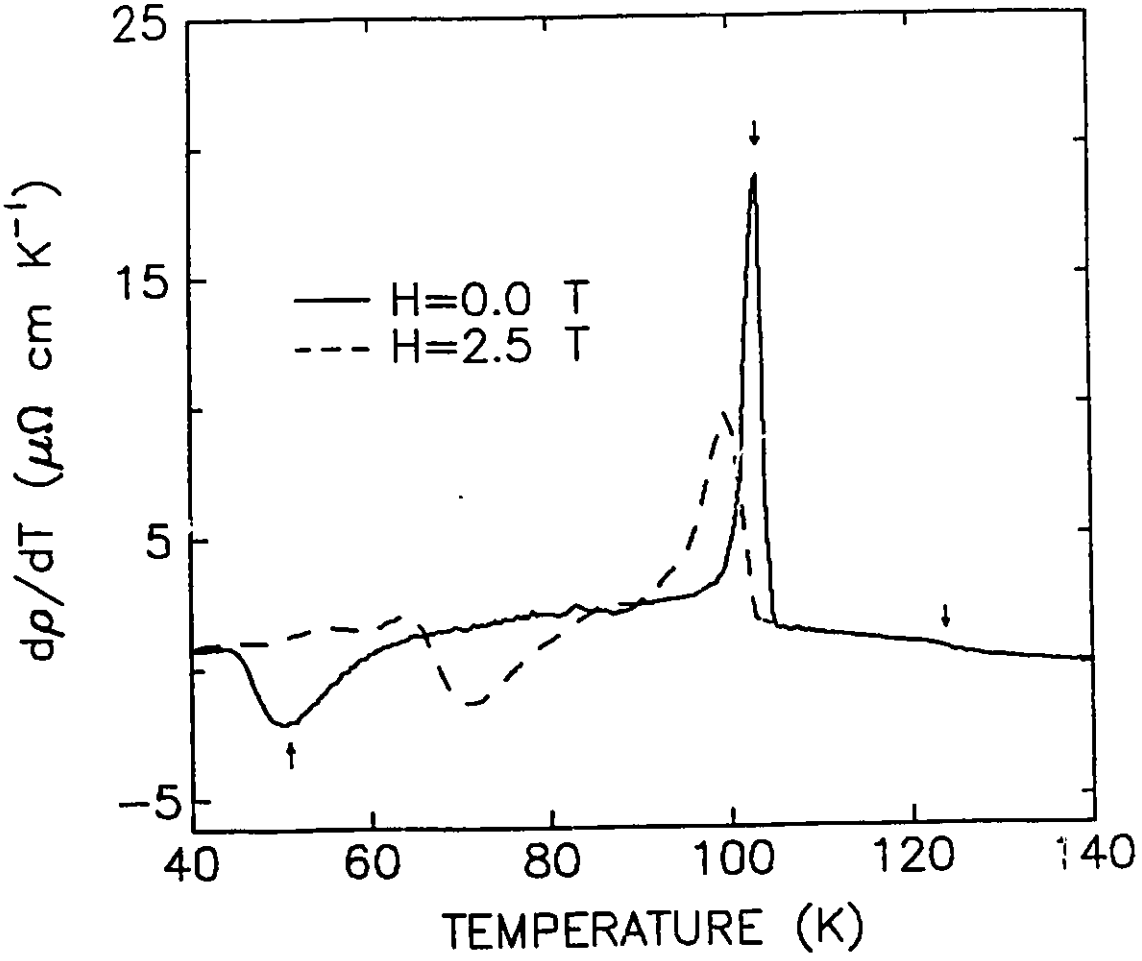
25
15
5
−5
40
60
80
100
120
140
H=0.0 T
H=2.5 T
dρ/dT (μΩ cm K⁻¹)
TEMPERATURE (K)

Figure 4.8

Phase diagram of UNi_2Si_2 mapped out through monitoring the field dependence of the transition temperatures. The dotted line is the result of neutron scattering measurements of Lin et al. (Lin et al, 1990). The triangle region on the left of the dotted line has the same LSDW (C) phase.

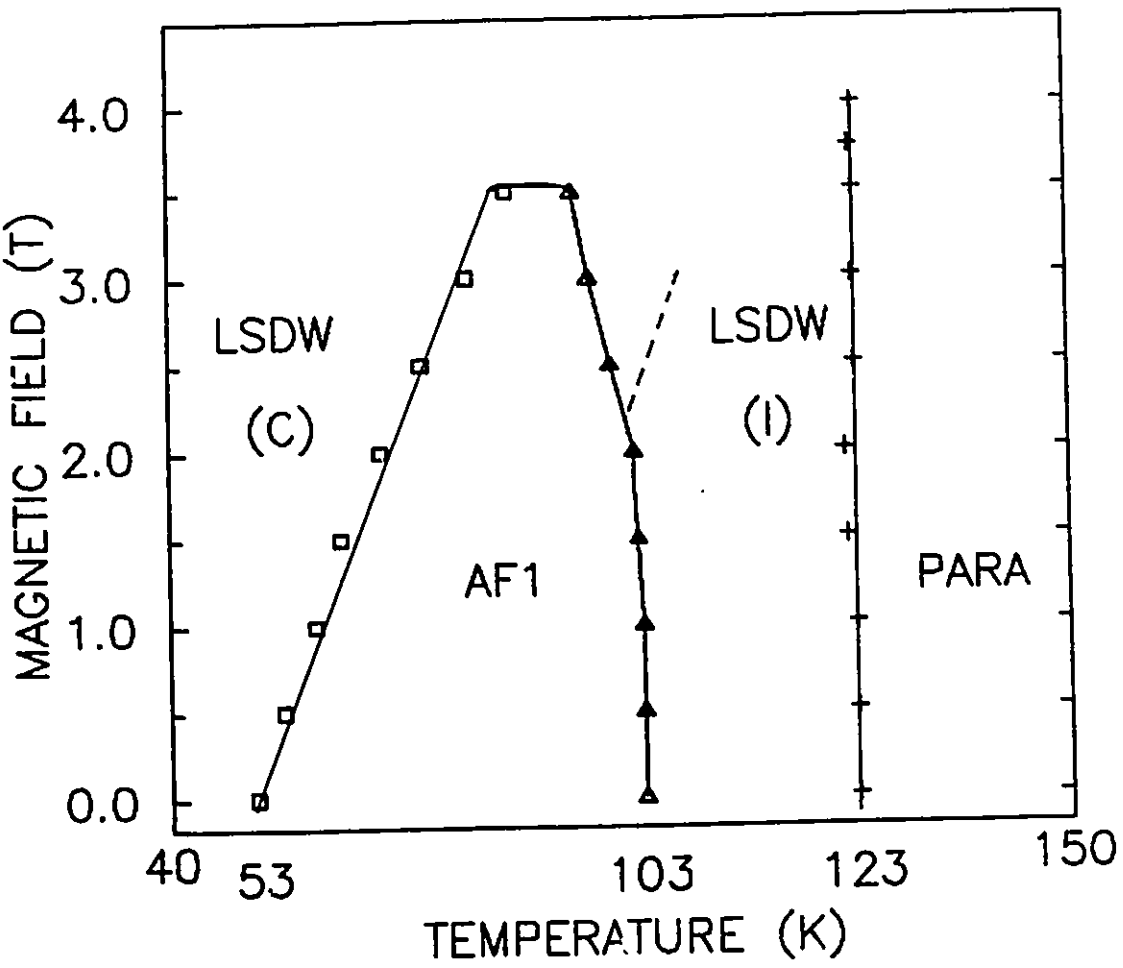
4.0
3.0
2.0
1.0
0.0
MAGNETIC FIELD (T)
LSDW
(C)
AF1
LSDW
(I)
PARA
40
53
103
123
150
TEMPERATURE (K)

The fact that the transitions are not seen in the resistivity measurements above 3.5 Tesla indicates that the LSDW⟷AF1 transitions do not occur above 3.5 Tesla and the lines around the AF1 region are connected in Figure 4.8. The increase of the LSDW⟷AF1 transition temperature with the applied magnetic field is expected, as the LSDW state gains certain energy by having the net moments aligned along the direction of the applied field. Similarly, such an argument can also be applied to explain the increase of the LSDW(C)⟷LSDW(I) transition temperature (see the dashed line).

4.6 Thermoelectric Power

The temperature dependence of the thermoelectric power of UNi_2Si_2 parallel ($S_{/}$) and perpendicular ($S_{\perp}$) to the tetragonal c axis is shown in Figure 4.9. The thermoelectric power is also anisotropic, with a larger magnitude perpendicular to the c axis. Above 123 K, both $S_{/}$ and $S_{\perp}$ are weakly temperature dependent and the ratio of $S_{\perp}/S_{/}$ is in the range of 2 - 4. The thermoelectric power is negative from room temperature down to about 20 K, and becomes positive at temperatures below 20 K. The positive thermoelectric power reaches a shallow but notable maximum at about 10 K and then starts to diminish as the temperature is lowered further. For the thermoelectric power perpendicular to the c axis, there is a broad peak centred at approximately 94 K. However, the only sharp feature associated with the phase transitions is the

Figure 4.9

Temperature dependence of the thermoelectric power of UNi_2Si_2.

▲: $\nabla T \parallel c$; □: $\nabla T \perp c$.

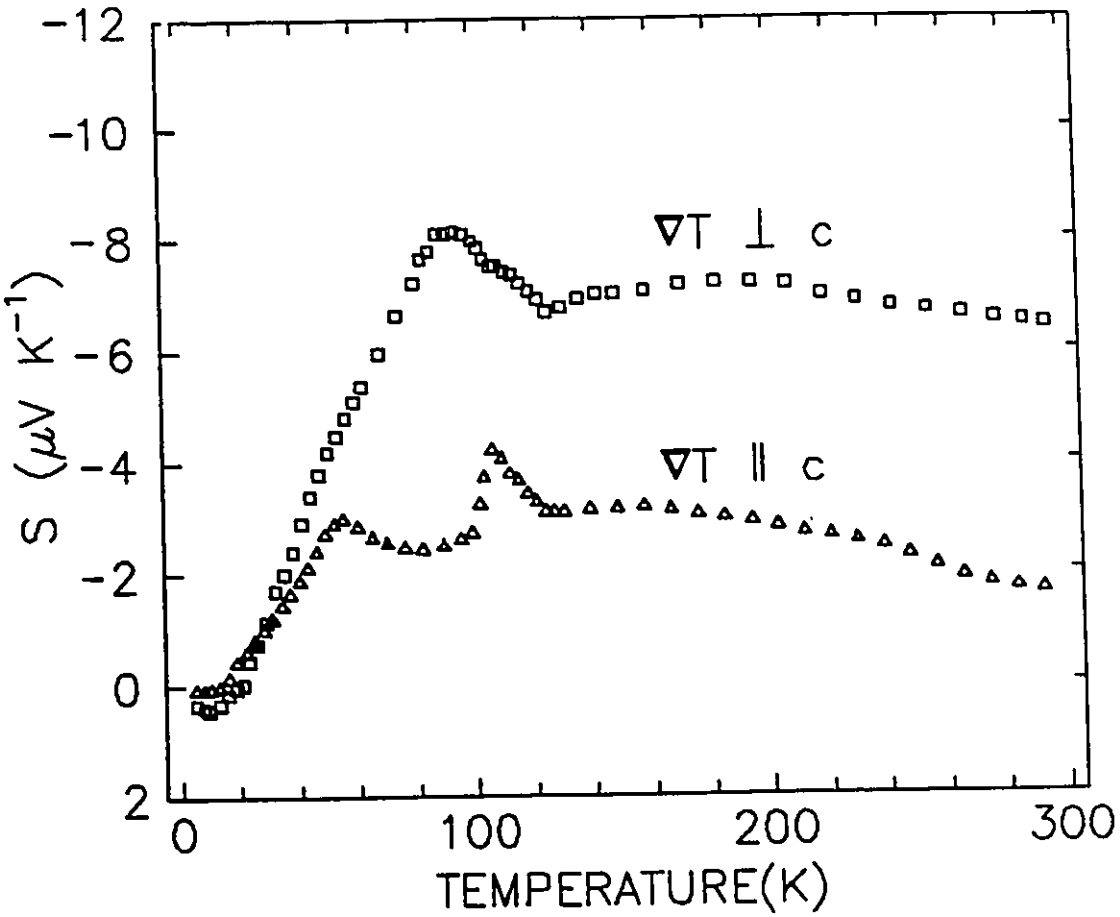
-12
-10
-8
-6
-4
-2
0
2
S (μV K^{-1})
$\nabla T \perp c$
$\nabla T \parallel c$
0
100
200
300
TEMPERATURE(K)

sudden increase of the magnitude at about 123 K. The features associated with the two phase transitions at lower temperatures, particularly the one at 53 K are rather weak compared with those observed in $S_{/}$. In fact, a feature as small as the one at 53 K in $S_{\perp}$ can easily come from a small (~ 5 degrees) sample mis-alignment. Thus, the behaviour of the thermoelectric power is in good correspondence with that of the resistivity in which $\rho_{/}$ shows distinct features at all three phase transitions while $\rho_{\perp}$ shows no feature at 53 K.

The fact that the thermoelectric power $S_{\perp}$ shows a very weak feature at 53 K transition together with the fact that the resistivity $\rho_{\perp}$ shows no feature at 53 K, suggest that the transport electrons moving in the basal plane ($\perp$c) are rather insensitive to the phase transition at 53 K. On the other hand, both the resistivity and thermopower parallel to the c axis show strong features at the 123 K and 103 K transitions as well as the 53 K transition. This may also be understood within the frame of a modified Fermi surface below 53 K already discussed in section 4.4, as such a modification can affect all of the transport properties.

4.7 Hall Effect

Figure 4.10 presents the temperature dependence of the Hall coefficient measured in a field of 1.6 Tesla. As in many of the Kondo lattice and heavy fermion compounds, the Hall coefficient of UNi_2Si_2 is positive except at its minimum where

Figure 4.10

Temperature dependence of the Hall coefficient of UNi_2Si_2 measured in a field of 1.6 Tesla. ▲: $H \| c$, $I \perp c$. □: $H \perp c$, $I \| c$.

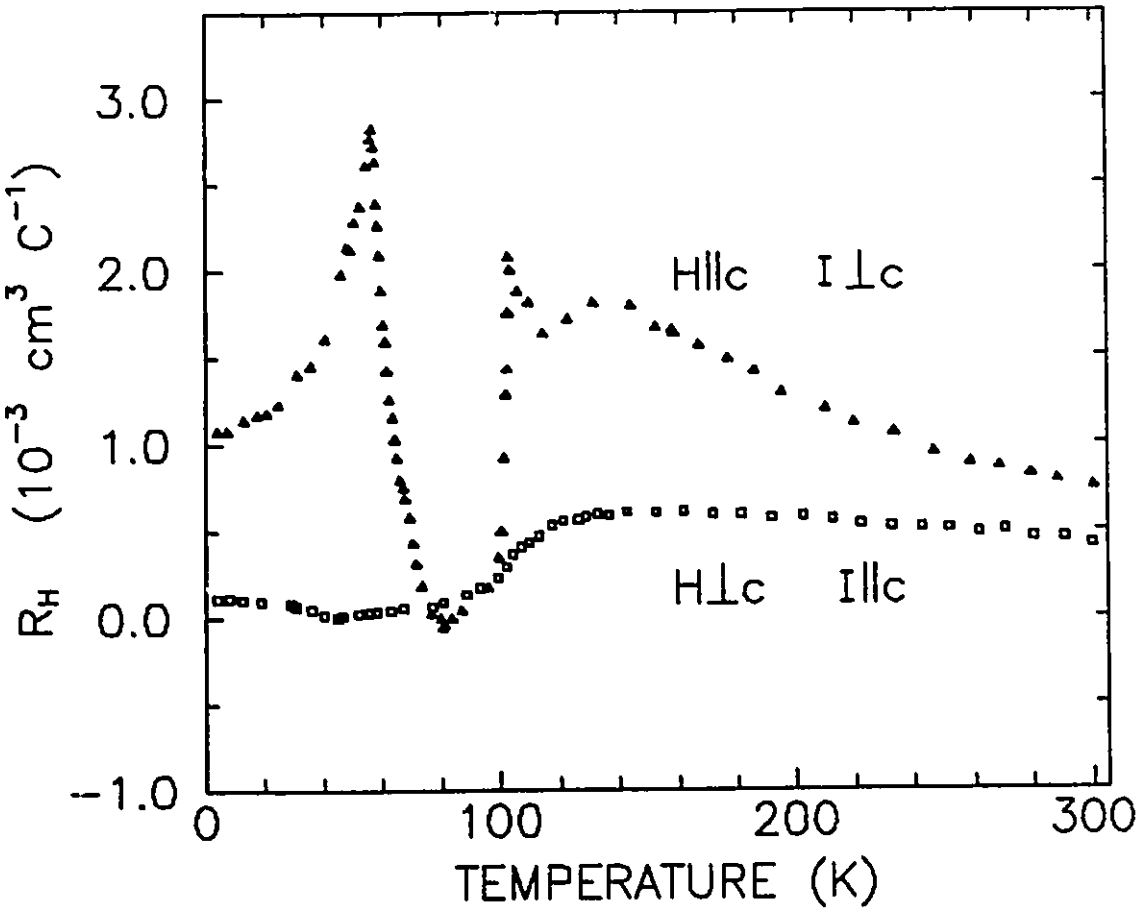
3.0
2.0
1.0
0.0
-1.0
R_H (10^{-3} cm^3 C^{-1})
H∥c I⊥c
H⊥c I∥c
0
100
200
300
TEMPERATURE (K)

small negative values are observed. Again, the behaviour of the Hall coefficient is very anisotropic in both magnitude and the temperature dependence.

We first focus on the Hall coefficient measured with $H \| c$ and $I \perp c$. The Hall coefficient gradually increases upon cooling from room temperature down to about 130 K. In the region of the incommensurate LSDW phase, a small dip in the Hall coefficient is developed. Between 103 and 56 K (the AF1 state), a giant U-shape dip is observed which yields sharp peaks at 103 and 56 K, respectively. Below 56 K, the Hall coefficient decreases monotonically. The Hall efficient measured with $H \perp c$ and $I \| c$ also shows a gradual increase with decreasing temperature down to about 130 K. Below 130 K, the Hall coefficient falls steadily to small values.

With the presence of skew scattering, the Hall coefficient can be written as:

$$R_H = R^o_H + R^s \rho_M(T) \chi(T) \qquad (4.4)$$

where R^o_H is the ordinary Hall coefficient, and R^s is the pre-factor of the skew scattering term and is related to phase shifts. In order to carry out a best fit of the Hall coefficient with the expression (4.4), one needs to know the magnetic part of the resistivity $\rho_M(T)$. An ideal approach would be to approximate the phonon part of the resistivity with the resistivity of $ThNi_2Si_2$, as such a compound is isostructural with UNi_2Si_2 and yet thorium contains no magnetic moment. However, since the phonon contribution to the

resistivity is small (14% as is estimated in section 4.3), it is a reasonable first approximation to replace $\rho_M(T)$ with the total resistivity. As we do not know how much of the residual resistivity ρ_o is due to magnetic scattering, we simply let ρ_o vary and be determined by the best fit. The best fit obtained is shown in Figure 4.11a as the solid line and the best-fit parameters are shown in Table 4.2.

For the case $H \perp c$ and $I \parallel c$, although the best fit and the experimental result has some discrepancies in the minimum region and in the region between 103 and 200 K, the overall features of the measured Hall coefficient are well accounted for by the theoretical model with single parameters R_H^o and R^s. For the case $H \perp c$ and $I \parallel c$, however, the experimental result cannot be satisfactorily accounted for by the model with fixed parameters R_H^o and R^s over the whole temperature range. Instead, it has to be broken into two separate regions, above and below T_c=53 K, to have a satisfactory fit of the data. The best fit so carried out is shown as the solid line in Figure 4.11b and the best-fit parameters are summarized in Table 4.2. As has been discussed in section 2.7 of Chapter 2, the sign and value of R^s depends sensitively on the phase shifts δ_i. It is therefore not surprising that R^s changes both its sign and value at the 53 K transition, as the form of the scattering potentials for transport electrons along the c axis may well be very different in the two ordered phases. On the other hand, the very different values of R_H^o below and above T_c, seem

Figure 4.11

Temperature dependence of the Hall coefficient measured in a field of 1.6 Tesla. (a): $H \| c$ and $I \perp c$; (b): $H \perp c$ and $I \| c$. The solid line is the best fit using the expression of $R_H = R_H^o + R^s \rho_M \chi$. The best-fit parameters are summarized in Table 4.2.

(a)

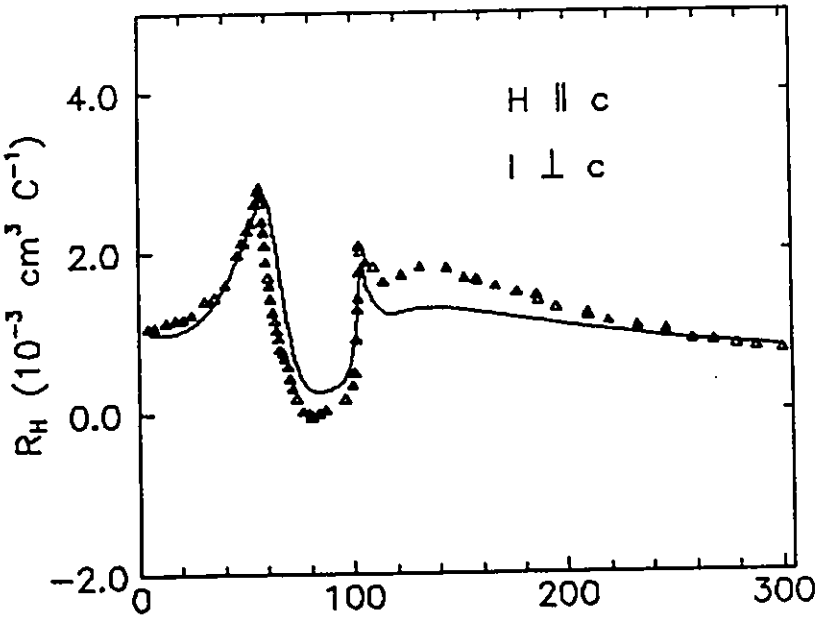
4.0
2.0
0.0
−2.0
0
100
200
300
H ∥ c
I ⊥ c
R_H (10^{-3} cm^3 C^{-1})

(b)

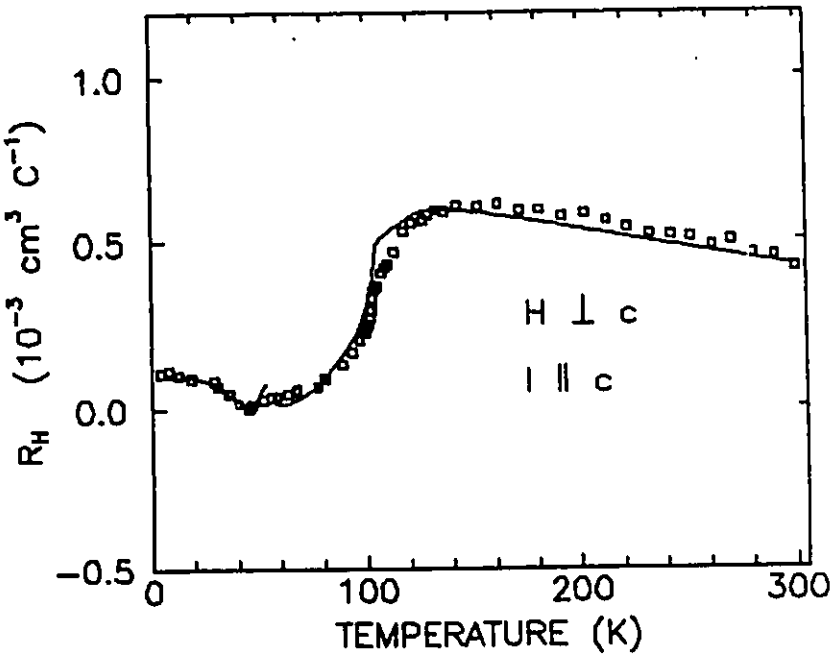
1.0
0.5
0.0
−0.5
0
100
200
300
H ⊥ c
I ∥ c
R_H (10^{-3} cm^3 C^{-1})
TEMPERATURE (K)

	Temp. Range	ρ_o ($\mu\Omega$ cm)	R_H^o (10^{-3} cm^3/C)	R^s ($10^3 \frac{cm^2\ mol}{\Omega\ C\ emu}$)
H∥c, I⊥c	4.2-300K	4.5	-0.03±0.03	1.4±0.1
H⊥c, I∥c	4.2-53K	3.5	0.10±0.01	-0.30±0.05
H⊥c, I∥c	53-300K	3.5	-0.05±0.01	1.59±0.04

Table 4.2. Parameters obtained through the best-fitting procedure of the Hall coefficient with the expression of $R_H = R_H^o + R^s \rho_H \chi$.

to imply a modification of the Fermi surface which is consistent with the anomalous increase in ρ, just below T_c.

4.8 Specific Heat

The specific heat of UNi_2Si_2 has been measured from 1.5 K to 29 K. The result is plotted as C_p/T versus T^2 in Figure 4.12. For T < 10 K, the data are fitted with the expression

$$C_p/T = \gamma_o + \beta T^2 \qquad (4.5)$$

where γ_o is the coefficient of the electronic term and β the coefficient of the cubic term (see inset of Figure 4.14). The fit yields γ_o = 21.8 ± 0.1 mJ mol^{-1} K^{-2} and β =0.0390 ± 0.0004 mJ mol^{-1} K^{-4}. The magnon contribution to the specific heat is expected to have an exponential behaviour when an energy gap is present in the magnon spectrum. However, such a behaviour is not observed in the specific heat which suggests that the magnon contribution is not significant at low temperatures. Assuming that the cubic term is a phonon contribution, a Debye temperature of θ_D=370 K is deduced from the β value . The small γ_o value extrapolated suggests a rather small mass enhancement in this system, hence one can conclude that UNi_2Si_2 is not a heavy Fermion material.

Figure 4.12

Specific heat divided by temperature (C_p/T) versus temperature squared (T^2) for UNi_2Si_2. The inset shows the linear fit of the low temperature part (1.5-10 K).

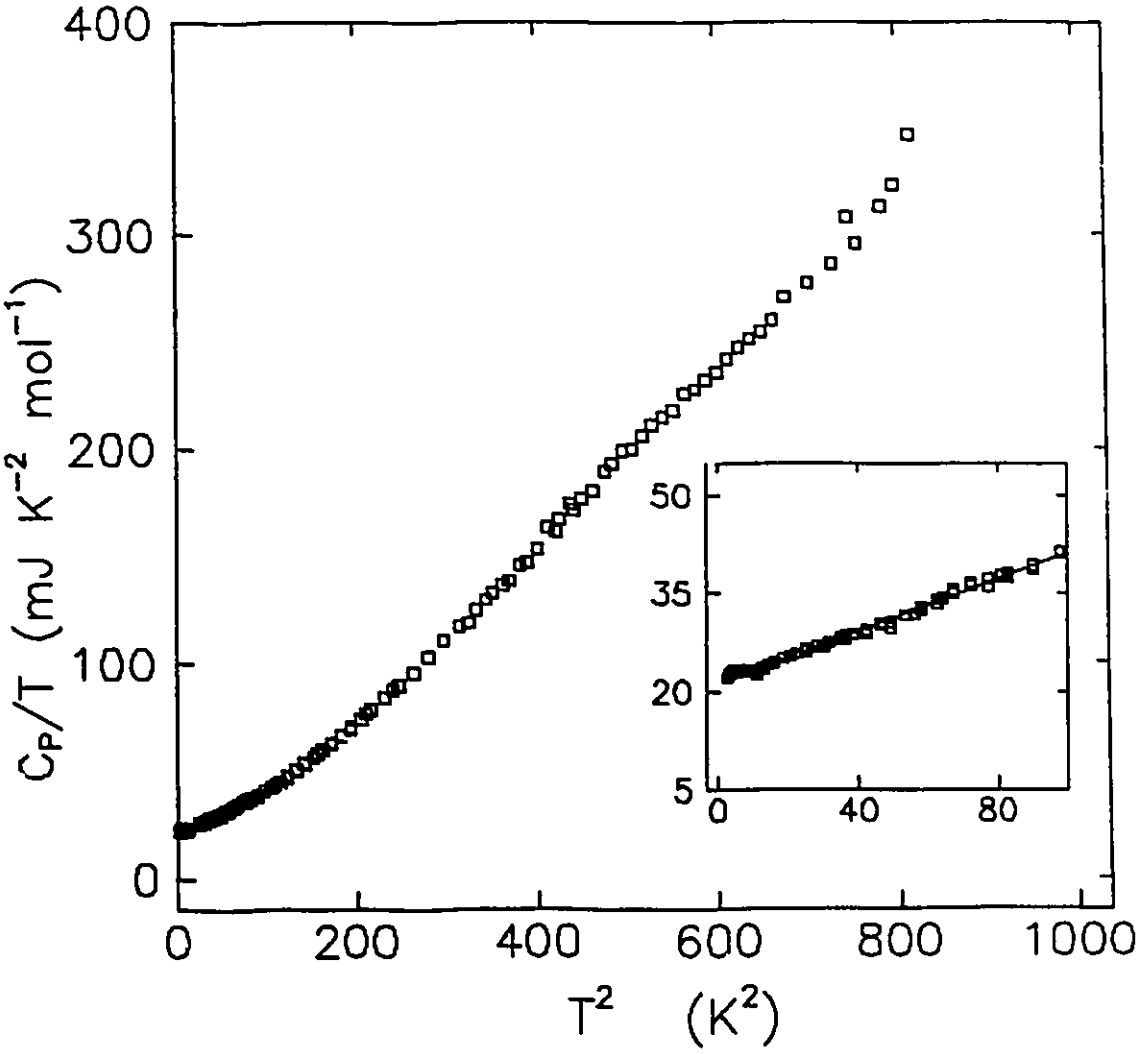
400
300
200
100
0
C_P/T (mJ K^{-2} mol^{-1})
0
200
400
600
800
1000
T^2 (K^2)
50
35
20
5
0
40
80

CHAPTER 5

UNi_2Ge_2

5.1 Introduction

UNi_2Ge_2 has the $ThCr_2Si_2$ type of structure and has been studied previously by neutron diffraction, magnetization and resistivity measurements. The neutron diffraction studies (Chelmicki et al, 1985) concluded that UNi_2Ge_2 is a simple body centred antiferromagnet of collinear AF1 type below T_N=74 K. The moments are associated with the uranium atoms and are aligned along the c axis in the ordered state. The magnetization measurements by both Chelmicki et al. and Dirkmaat show the typical behaviour of a simple antiferromagnet, although the latter has a slightly higher Néel temperature (77K). In addition to the magnetization measurement, Dirkmaat (Dirkmaat, 1989) also measured the resistivity of UNi_2Ge_2 which shows a nearly temperature-independent behaviour above T_N and fast decrease below T_N . In fact, the decrease was found to follow a T^2 dependence below 30 K. These measurements were all performed on polycrystalline samples and no detailed study of the anisotropies of the physical properties in this system was reported up to this point.

5.2 Sample Preparation

The single crystal of UNi_2Ge_2 used in this study was prepared from U, Ni, and Ge ingots with exactly the same procedures for preparing single-crystal UNi_2Si_2 described in section 4.2 of Chapter 4. The samples were cut parallel and perpendicular to the tetragonal c axis with a spark cutter. X-ray measurements indicated that the samples were single crystals with lattice parameters of a=4.09 Å and c=9.47 Å.

5.3 Magnetic Susceptibility

Figure 5.1 shows the temperature dependence of the magnetic susceptibility (M/H) measured in a field of 1.5 Tesla with the fields applied parallel ($\chi_{\parallel}$) and perpendicular ($\chi_{\perp}$) to the c axis. The ratio of $\chi_{\parallel}/\chi_{\perp}$ is 1.2 at room temperature and is about 0.3 at 5 K. The susceptibility is Curie-Weiss like at higher temperatures, as can be seen from the inverse susceptibility shown in Figure 5.2. A best fit above 85 K with the expression

$$\chi=C/(T-\theta_{CW}) \qquad (5.1)$$

yields μ_{eff} =3.05 μ_B, θ_{CW}=-2.3 K for $\chi_{\parallel}$, and μ_{eff}=3.09 μ_B, θ_{CW}=-79 K for $\chi_{\perp}$. The large anisotropy in the Curie-Weiss temperature θ_{CW} suggests a strong confinement of the moments along the c axis. The susceptibility starts to deviate from the Curie-Weiss behaviour at about 85 K. At about 77 K, a peak characteristic of an antiferromagnetic phase transition occurs in $\chi_{\parallel}$ while a change of slope in $\chi_{\perp}$ is seen. The shoulders at

Figure 5.1

Temperature dependence of the magnetic susceptibility of UNi_2Ge_2 measured in a field of 1.5 Tesla. ▲: H∥c; □: H⊥c.

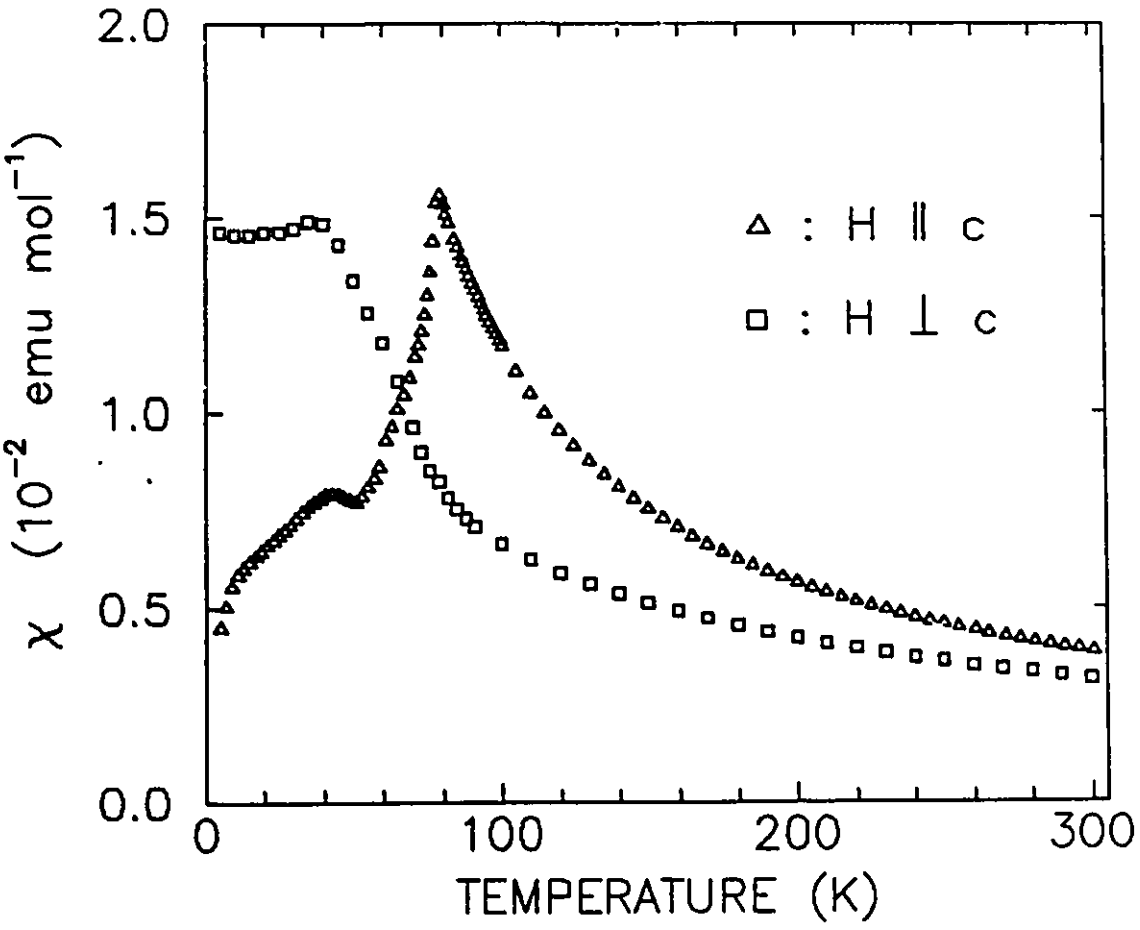
2.0
1.5
1.0
0.5
0.0
χ (10⁻² emu mol⁻¹)
△ : H ∥ c
□ : H ⊥ c
0
100
200
300
TEMPERATURE (K)

Figure 5.2

Temperature dependence of the inverse susceptibility of UNi_2Ge_2 measured in a field of 1.5 Tesla. ▲: $H \| c$; □: $H \perp c$.

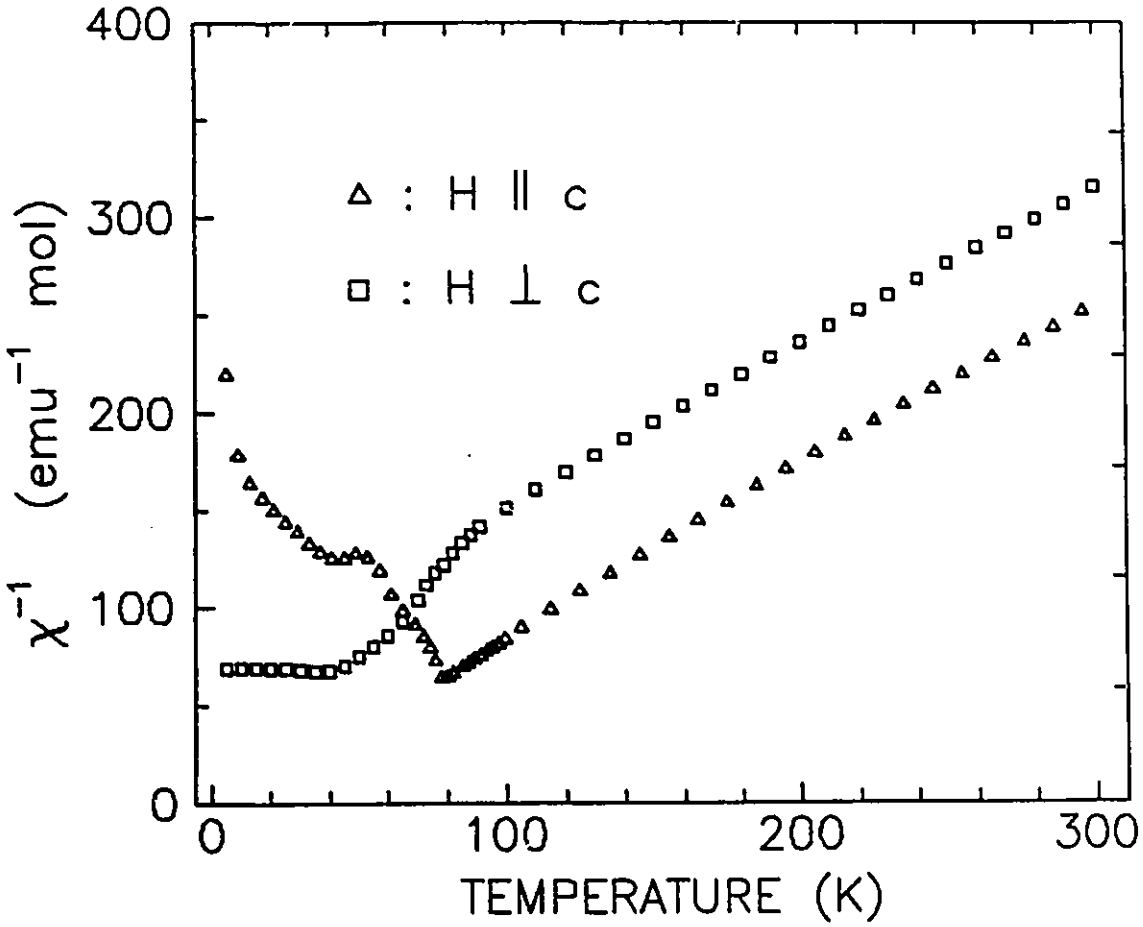
400
300
200
100
0
χ^{-1} (emu^{-1} mol)
△ : H ∥ c
□ : H ⊥ c
0
100
200
300
TEMPERATURE (K)

about 50 K are due to the presence of a weak ferromagnetism which sets in together with the antiferromagnetic ordering at about 77 K.

The clear evidence of the weak ferromagnetism comes from the hysteresis in the field dependence of the magnetization at 5 K, as is shown in Figure 5.3a. Figure 5.3b shows the decay of the magnetization in zero magnetic field (see figure caption for detail) with increasing temperature. Such a behaviour also exists in the magnetization perpendicular to the tetragonal c axis. At 5 K, the ferromagnetic moment perpendicular to the c axis is about twice as large as the one along the c axis.

The ferromagnetic component is very weak indeed. The effective moment estimated at 5 K in a field of 1.5 Tesla is only a few percent of a Bohr magneton per U atom. Such a ferromagnetic moment is too small to be picked up by a neutron scattering experiment in the presence of the large uranium moments. This may explain why no ferromagnetism has been reported in previous neutron work on powder samples. The behaviour of the weak ferromagnetism is quite peculiar and cannot be explained by a simple canted antiferromagnetic structure, as such a structure does not give rise to the weak ferromagnetism observed perpendicular to the c axis. In fact, the tetragonal structure of UNi_2Ge_2 has the central inversion symmetry which does not allow a canted antiferromagnetic structure (Moriya 1963). Neither can it be explained by the

Figure 5.3

(a) Magnetic hysteresis of the magnetization of UNi_2Ge_2 measured at 5 K. The field is applied along the c axis.
(b) Decay of the magnetization of UNi_2Ge_2 with increasing temperature. The sample first was aligned with a 5 Tesla field along the c axis at 5 K. The moment was then measured along the c axis in a zero applied magnetic field.

(a)

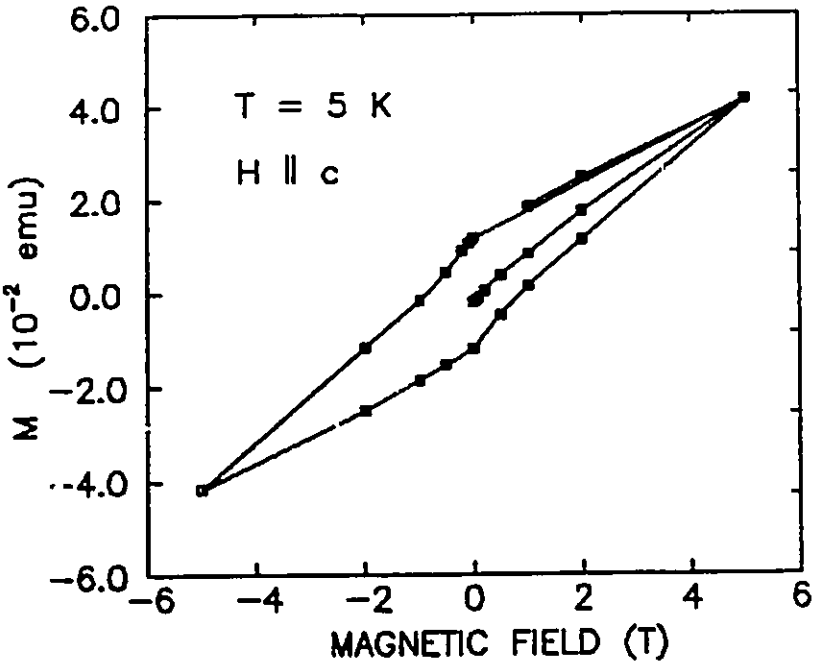
T = 5 K
H ∥ c
M (10⁻² emu)
MAGNETIC FIELD (T)
6.0
4.0
2.0
0.0
-2.0
-4.0
-6.0
-6
-4
-2
0
2
4
6

(b)

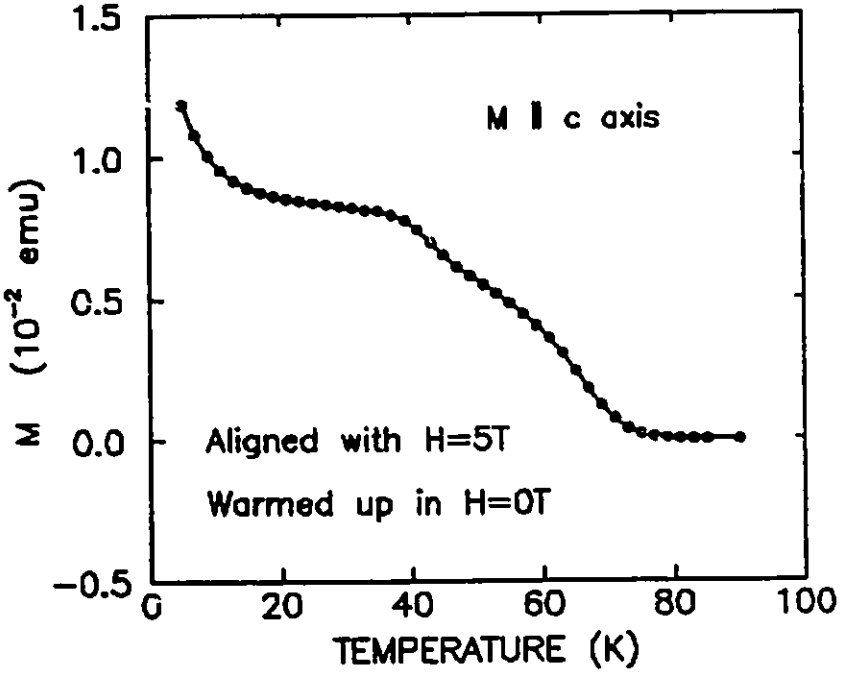
M ∥ c axis
Aligned with H=5T
Warmed up in H=0T
M (10⁻² emu)
TEMPERATURE (K)
1.5
1.0
0.5
0.0
-0.5
0
20
40
60
80
100

presence of any ferromagnetic impurity as the weak ferromagnetism sets in together with the antiferromagnetic ordering at the Néel temperature T_N. It is speculated that some kind of imperfection of the sample is somehow responsible for the weak ferromagnetism observed. However, detailed knowledge of the crystal structure below the Néel temperature is needed before one can proceed further.

5.4 Electrical Resistivity

The dc resistivity of UNi_2Ge_2, both parallel ($\rho_{/\!/}$) and perpendicular ($\rho_\perp$) to the c axis, has been measured from 4.2 to 300 K. The result is shown in Figure 5.4. Again, the resistivity is very anisotropic. The room-temperature value of the resistivity is 317 $\mu\Omega$ cm for $\rho_{/\!/}$ and is 178 $\mu\Omega$ cm for $\rho_\perp$. At 4.2 K, the value of $\rho_{/\!/}$ is 203 $\mu\Omega$ cm and that of $\rho_\perp$ is only 7.8 $\mu\Omega$ cm. Similar to UNi_2Si_2, the temperature dependence of the resistivity is relatively weak above the Néel temperature T_N, with a positive coefficient $d\rho/dT$ for $\rho_\perp$ and a negative coefficient for $\rho_{/\!/}$. Below the Néel temperature, the resistivity $\rho_\perp$ decreases drastically with decreasing temperature while the resistivity $\rho_{/\!/}$ shows an anomalous increase just below the Néel temperature T_N, reaching a giant maximum of 668 $\mu\Omega$ cm at about 60 K, decreasing at lower temperatures.

The resistivity $\rho_{/\!/}$ has the negative slope characteristic of Kondo behaviour above the Néel temperature T_N. Between 125 and 300 K, $\rho_{/\!/}$ can be fitted with the

Figure 5.4

Temperature dependence of the resistivity of UNi_2Ge_2 with the current parallel and perpendicular to the c axis.

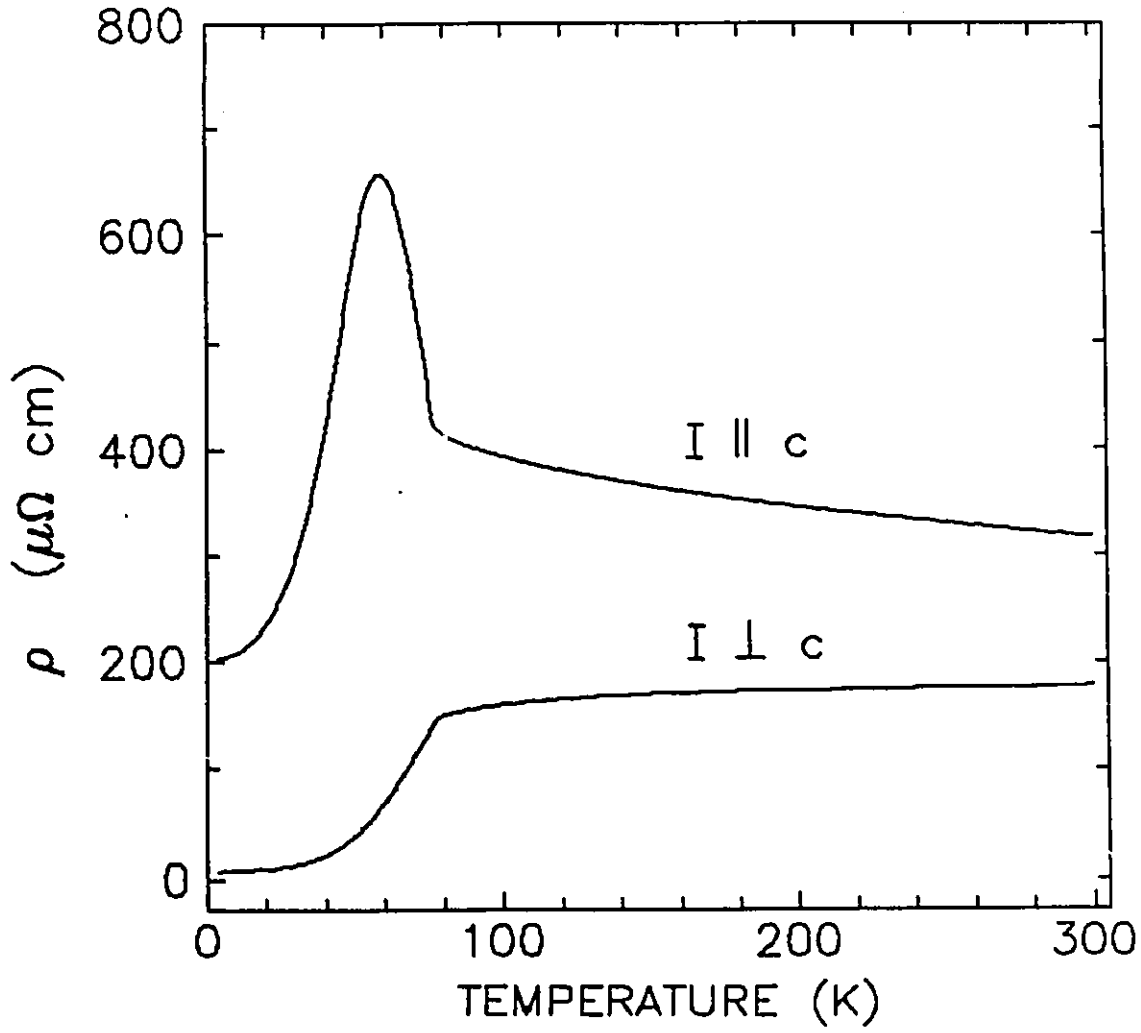
800
600
400
200
0
ρ (μΩ cm)
I ∥ c
I ⊥ c
0
100
200
300
TEMPERATURE (K)

expression

$$\rho = \rho_o + AT - B\ln T \qquad (5.2)$$

for temperatures above 125 K, as is shown in Figure 5.5. The best fit parameters obtained are: ρ_o=689 $\mu\Omega$ cm, A=0.027 $\mu\Omega$ cm K^{-1} and B= 63.7 $\mu\Omega$ cm $(\ln K)^{-1}$. The phonon resistivity at room temperature can be estimated from the value of A and is about 8 $\mu\Omega$ cm. Assuming the variation in $\rho_\perp$ well above the Néel temperature is due to electron-phonon scattering, as the spin-disorder scattering resistivity saturates, one obtains an estimated value of 14 $\mu\Omega$ cm for the phonon resistivity at room temperature. These numbers, although not to be taken too literally, clearly indicate that electron-phonon scattering is not the dominant scattering mechanism responsible for the large resistivity in this system.

Similar to the case of UNi_2Si_2, the resistivity of UNi_2Ge_2 at moderately low temperatures can be described by a gapped spin-wave term plus a T^2 term:

$$\rho = \rho_o + AT^2 + BT(1+2T/\Delta)\exp(-\Delta/T) \qquad (5.3)$$

The best fit of the resistivity with this model is shown in Figure 5.6. The best-fit parameters, together with the temperature range of fitting, are summarized in Table 5.1. It is worth noting that the gap values for UNi_2Si_2 and UNi_2Ge_2 are all roughly around 100 K, indicating a similar magnetic anisotropy in the two systems.

The most remarkable feature of the resistivity is perhaps the giant maximum in $\rho_\parallel$ below the Néel temperature.

Figure 5.5

Resistivity of UNi_2Ge_2 with $I \| c$ in the temperature range of 100-300 K. The solid line is the best fit with the expression of $\rho = \rho_o + AT - B\ln T$. Some of the data points have been removed for clarity.

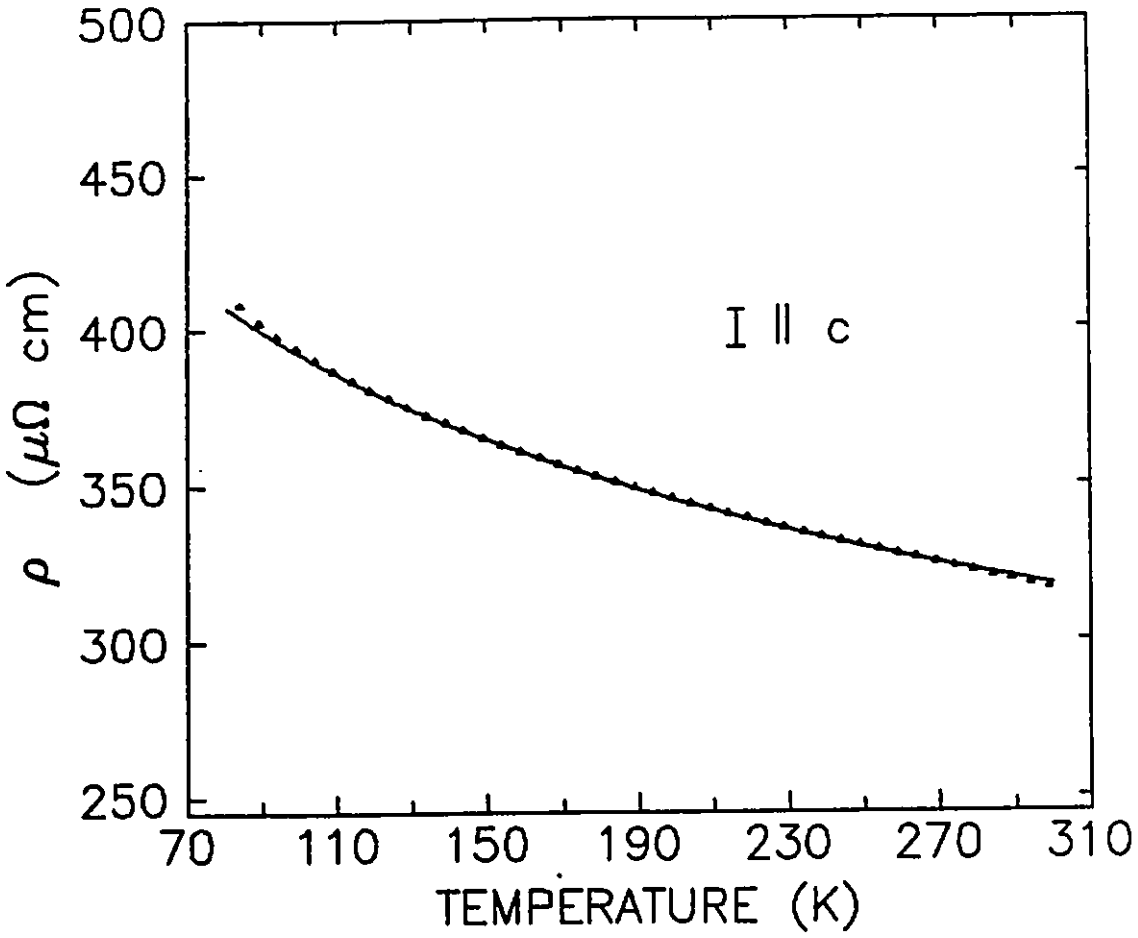
500
450
400
350
300
250
ρ (μΩ cm)
I ∥ c
70
110
150
190
230
270
310
TEMPERATURE (K)

Figure 5.6

Resistivity of UNi_2Ge_2 in the temperature range of 4.2-45 K. (a) $I \| c$; (b) $I \perp c$. The solid line is the best fit using the expression of $\rho = \rho_o + AT^2 + BT(1+2T/\Delta)\exp(-\Delta/T)$. The best-fit parameters are summarized in Table 5.1. Some of the data points have been removed for clarity.

(a)

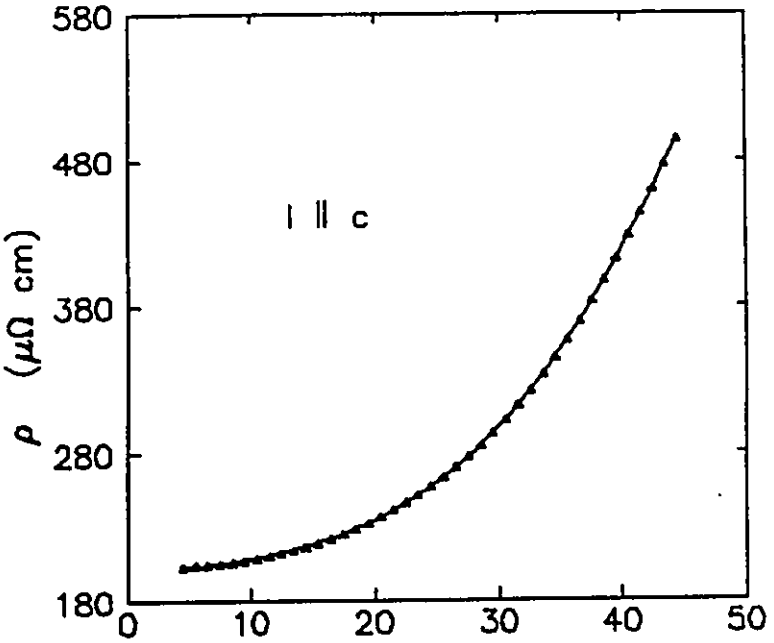
580
480
380
280
180
ρ (μΩ cm)
I ∥ c
0
10
20
30
40
50

(b)

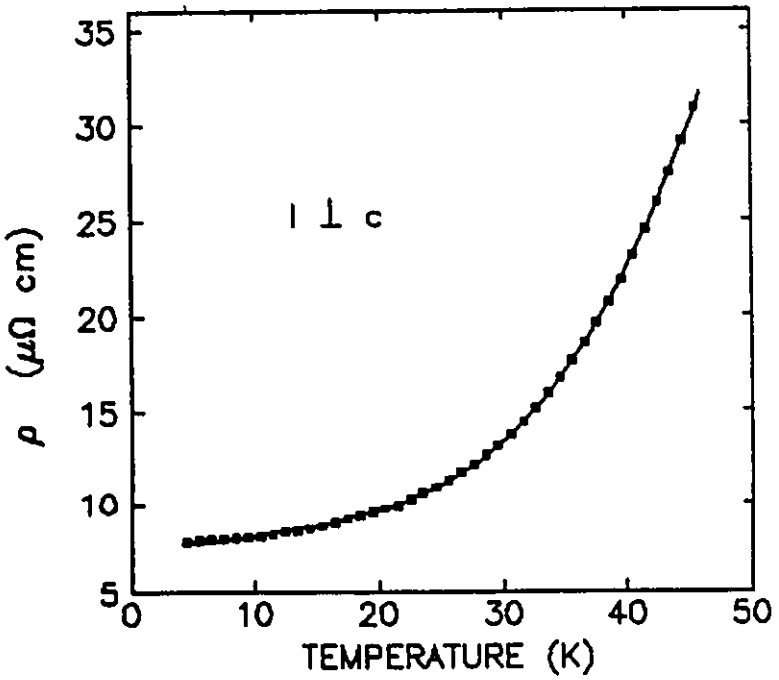
35
30
25
20
15
10
5
ρ (μΩ cm)
I ⊥ c
0
10
20
30
40
50
TEMPERATURE (K)

	Temp. Range	ρ_o ($\mu\Omega$ cm)	A ($\mu\Omega$ cm K^{-2})	B ($\mu\Omega$ cm K^{-1})	Δ (K)
I$\parallel$c	4.2-45K	201	0.0753	14.06	95
I$\perp$c	4.2-45K	7.6	0.0048	3.71	138

Table 5.1. Best-fit parameters obtained from fitting the low temperature resistivity of UNi_2Ge_2 with the expression of $\rho = \rho_o + AT^2 + BT(1+2T/\Delta)\exp(-\Delta/T)$.

This kind of resistivity maximum just below the Néel temperature has been seen in several systems including Cr, α-Mn, Dy (Meaden, 1965), and URu_2Si_2 (Palstra et al, 1986; Dawson et al, 1989). However, none of the above mentioned has the huge magnitude of the maximum seen in UNi_2Ge_2. The theoretical model used with some success in explaining this phenomenon has been the one first proposed by Miwa (Miwa, 1963) and later developed by Suezaki and Mori (Suezaki and Mori, 1969), as has been discussed in section 2.5 of Chapter 2. The expression given by this model for resistivity just below the Néel temperature is the following:

$$\rho_f - \rho(T_N) = A(T_N-T)^{0.33} - B(T_N-T)^{0.66} \qquad (5.4)$$

where the first term is the gap term and the second is the spin-fluctuation term. The exponents were determined for a 3d Ising model (Collins, 1989). The gapping of the Fermi surface is highly plausible, as the magnetic "Brillouin zone" is only half of the size of the lattice Brillouin zone and most of the zone-folding occurs along the c^* axis. In Figure 5.7, a theoretical curve generated using this expression with A=250 and B=65 is shown, together with the experimental data ρ_f. The agreement with the experiment is by no means satisfactory, but it does give rise to the same general feature of the resistivity anomaly below the Néel temperature.

5.5 Hall Effect

Figure 5.8 presents the temperature dependence of the

Figure 5.7

Resistivity anomaly in $\rho_{/\!/}$ of UNi_2Ge_2 below the Néel temperature T_N. The solid line is a theoretical curve generated using the expression $\rho = \rho(T_N) + A(T_N-T)^{0.33} - B(T_N-T)^{0.66}$ with A=250 and B=65.

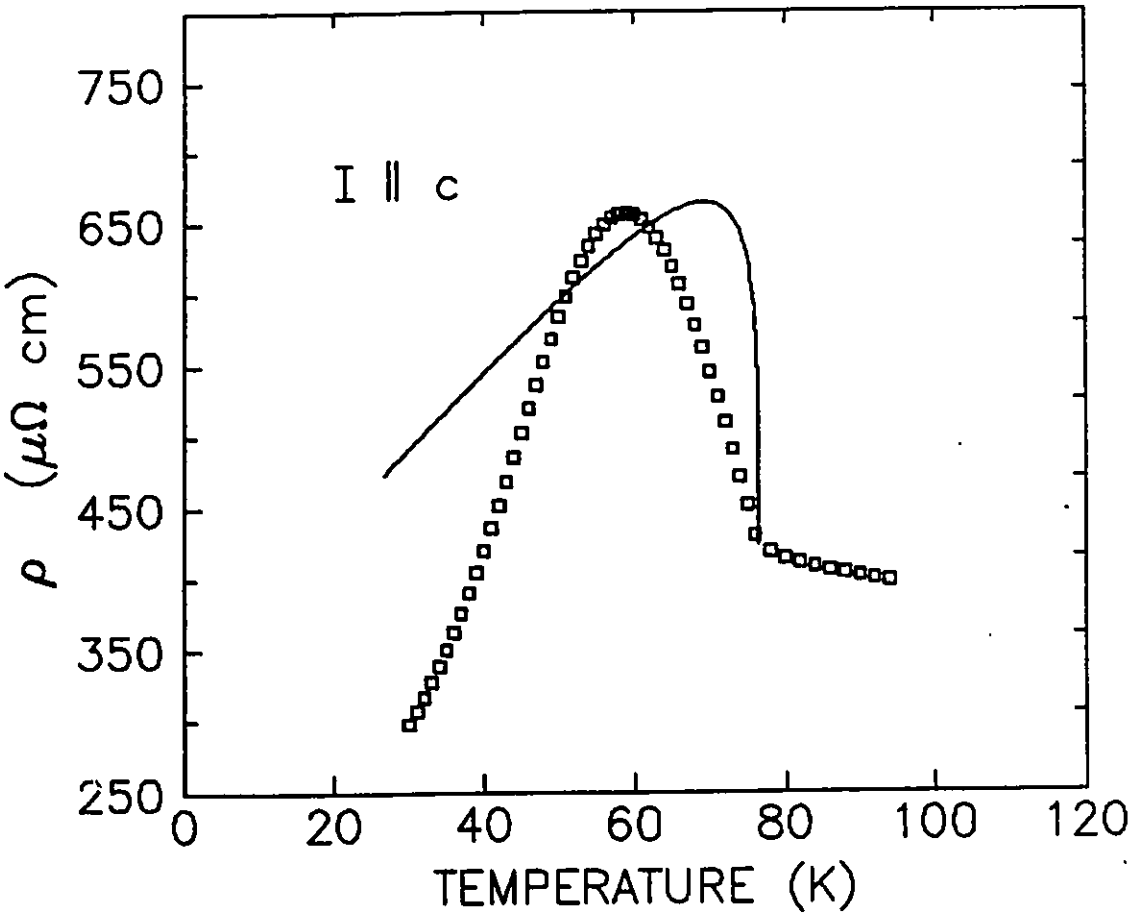
I ∥ c
ρ (μΩ cm)
750
650
550
450
350
250
0
20
40
60
80
100
120
TEMPERATURE (K)

Figure 5.8

Temperature dependence of the Hall coefficient of UNi_2Ge_2 measured in a field of 1.5 Tesla. ▲: H∥c, I⊥c. □: H⊥c, I∥c.

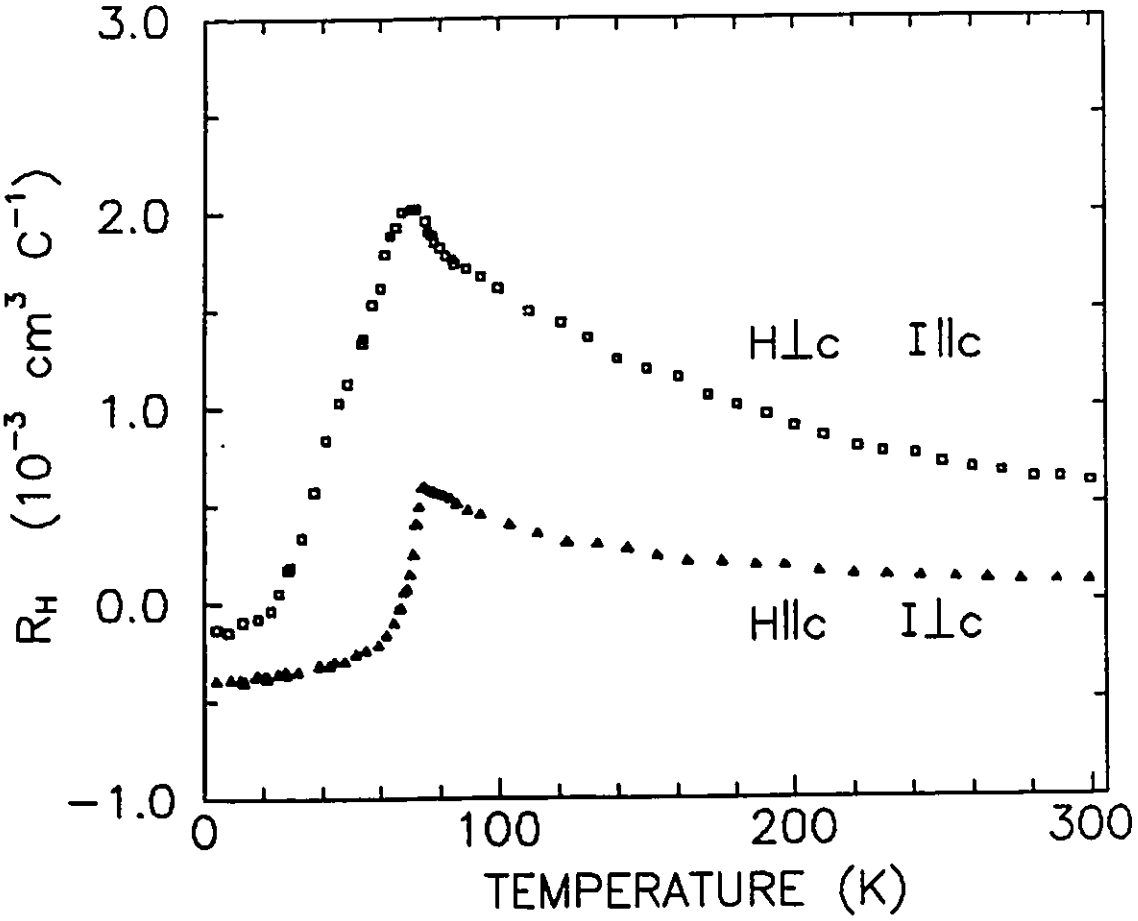
3.0
2.0
1.0
0.0
−1.0
R_H (10^{-3} cm^3 C^{-1})
0
100
200
300
TEMPERATURE (K)
H⊥c I∥c
H∥c I⊥c

Hall coefficient of UNi_2Ge_2 measured in a field of 1.5 Tesla. The Hall coefficient is positive at higher temperatures and shows a gradual increase with decreasing temperature. Below the Néel temperature, the Hall coefficient decreases drastically and becomes negative at low temperatures. Generally speaking, the Hall coefficient measured with $H \perp c$; $I \parallel c$ has a larger value (2-3 times) than that measured with $H \parallel c$; $I \perp c$ except at low temperatures where the latter is more negative than the former.

The temperature dependence of the Hall coefficient can be well accounted for by the model of Fert and Levy (Fert and Levy, 1987) which invokes the ordinary Hall effect and the skew-scattering contribution:

$$R_H = R_H^o + R^s \rho_M \chi \qquad (5.5)$$

In Figure 5.9a, the best fit with this model for the case $H \parallel c$; $I \perp c$ is shown as the solid curve over the entire temperature range measured. The procedure is exactly the same as described in section 4.6 of Chapter 4. The best-fit parameters are summarized in Table 5.2. Despite the small discrepancies at the low and high temperature ends, the fit is rather satisfactory. For the case $H \perp c$; $I \parallel c$, it is again necessary to break the data into two separate temperature regions, below and above the Néel temperature T_N, to fit the data satisfactorily with this model. The best fit is shown in Figure 5.9b as the solid line and the fitting parameters are summarized in Table 5.2.

Figure 5.9

Temperature dependence of the Hall coefficient measured in a field of 1.5 Tesla. (a) $H \| c$ and $I \perp c$; (b) $H \perp c$ and $I \| c$. The solid line is the best fit using the expression of $R_H = R_H^o + R^s \rho_M \chi$. The best-fit parameters are summarized in Table 5.2.

(a)

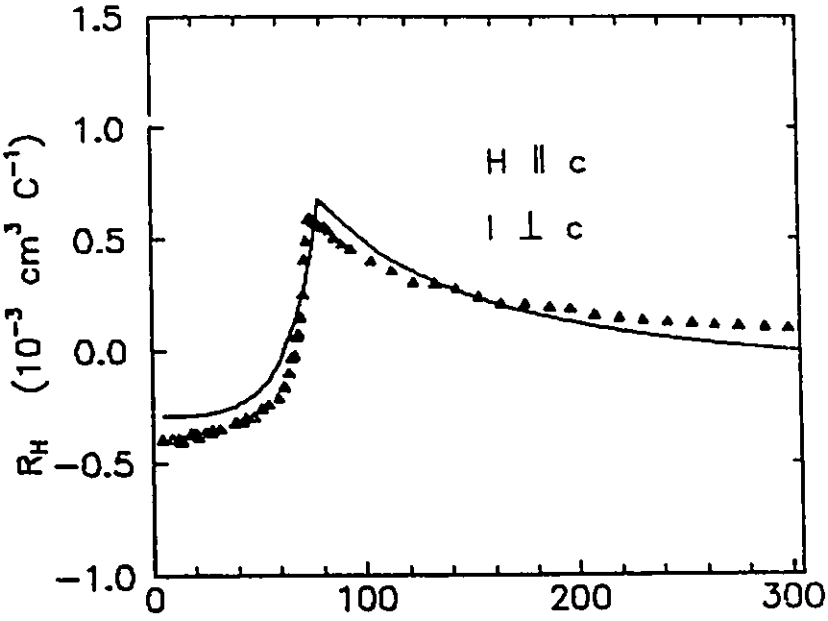
1.5
1.0
0.5
0.0
−0.5
−1.0
R_H (10^{-3} cm^3 C^{-1})
H ∥ c
I ⊥ c
0
100
200
300

(b)

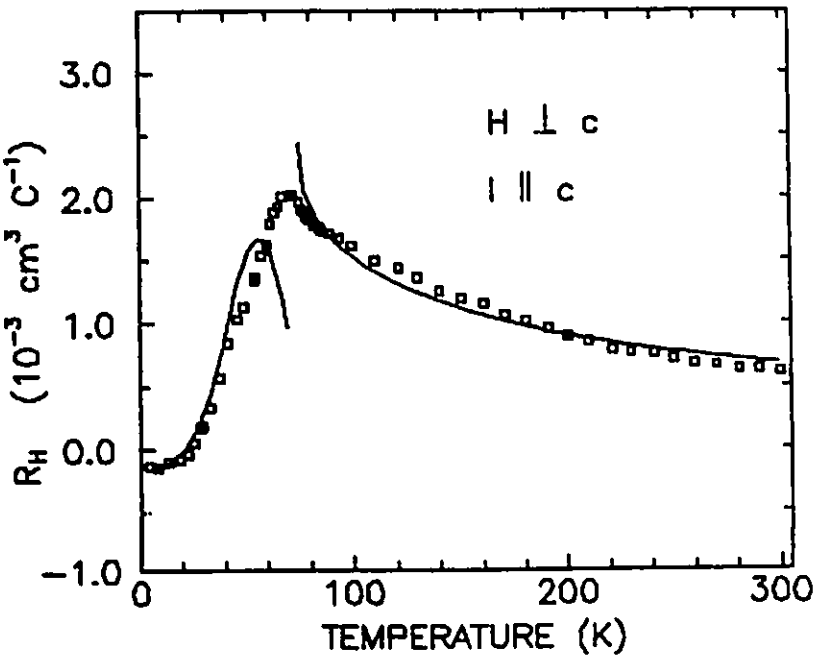
3.0
2.0
1.0
0.0
−1.0
R_H (10^{-3} cm^3 C^{-1})
H ⊥ c
I ∥ c
0
100
200
300
TEMPERATURE (K)

	Temp. Range	ρ_o ($\mu\Omega$ cm)	R_H^o (10^{-3} cm^3/C)	R^s ($10^3 \frac{cm^2\ mol}{\Omega\ C\ emu}$)
H∥c, I⊥c	4.2-300K	0.0	-0.30±0.01	0.44±0.01
H⊥c, I∥c	4.2-76K	3.0	-0.2±0.1	0.34±0.04
H⊥c, I∥c	76-300K	3.0	0.33±0.03	0.93±0.03

Table 5.2. Best-fit parameters obtained through fitting the Hall coefficient of UNi_2Ge_2 with the expression of $R_H = R_H^o + R^s\rho_M\chi$.

The necessity of separating the Hall coefficient into two regions to best fit the data for the case $H \perp c$ and $I \parallel c$ has profound implications. As discussed earlier in section 4.7 of Chapter 4, the very different values of R^s above and below the Néel temperature T_N perhaps should be best interpreted as due to the change of the scattering potentials. The change of the ordinary Hall coefficient R_H^o across the Néel temperature signals a modification of the Fermi surface due to the antiferromagnetic ordering. Such a result is also consistent with the anomalous increase of $\rho_\parallel$ just below T_N as it also requires a modification of the Fermi surface (gapping).

CHAPTER 6

CONCLUSIONS

Magnetic susceptibility, resistivity and the Hall coefficient of UNi_2Si_2 and UNi_2Ge_2 have been studied in detail. Thermoelectric power and specific heat measurements of UNi_2Si_2 have been carried out. The magnetic and transport properties of these two systems are highly anisotropic, with the transport properties strongly coupled to the magnetism in these systems.

The magnetic susceptibility of UNi_2Si_2 and UNi_2Ge_2 is Curie-Weiss like in the paramagnetic state at higher temperatures. For UNi_2Si_2, the effective moment per U-atom is 3.62 μ_B for H$\parallel$c and 3.55 μ_B for H$\perp$c. These numbers are very close to the calculated value of 3.62 μ_B for trivalent uranium. The Curie-Weiss temperature extrapolated from the experimental result is θ_{CW}=-15 K for H$\parallel$c and θ_{CW}=-530 K for H$\perp$c. At about 78 K, the onset of ferromagnetism is observed with the moment along the c axis. The ferromagnetic moment is about 0.62 μ_B per U-atom which is in reasonable agreement with the neutron diffraction result of 1.0 $\pm$ 0.3 μ_B (Lin et al, 1991). For UNi_2Ge_2, the effective moment per U-atom is 3.05 μ_B for H$\parallel$c and 3.09 μ_B for H$\perp$c which are less than the

calculated value of 3.62 μ_B for trivalent uranium. The Curie-Weiss temperature is θ_{CW}=-2.3 K for H$\parallel$c and θ_{CW}=-79 K for H$\perp$c. The Curie-Weiss temperatures of the two systems are quite different. However, if one compares the ratios of θ_{CW} parallel and perpendicular to the c axis of the two compounds, they are very similar indicating a similar magnetic anisotropy in these two systems. The behaviour of the weak ferromagnetism occurring in UNi_2Ge_2 is very peculiar and remains one of the unanswered questions at this stage of the study.

The resistivity of both UNi_2Si_2 and UNi_2Ge_2 is largely due to magnetic scattering of the conduction electrons. At room temperature, the phonon contribution to the resistivity is estimated to be only 14% for UNi_2Si_2 and 8% for UNi_2Ge_2. At high temperatures, the resistivity along the c axis shows a Kondo type of increase with decreasing temperature. However, only UNi_2Ge_2 can be described by the theoretical model satisfactorily. At low temperatures, the resistivity in both compounds can be described by a T^2 term plus a term due to gapped spin-wave scattering. The precise origin of the T^2 term is not clear yet. The magnon gap values obtained through the resistivity analysis are around 100 K which further demonstrates the similar magnetic anisotropy in these two compounds. The most remarkable features are the anomalous increase of the resistivity along the c axis associated with the 53 K transition in UNi_2Si_2 and the antiferromagnetic ordering in UNi_2Ge_2. Although there is a lack of a detailed

understanding, the resistivity anomaly, both in UNi_2Si_2 and UNi_2Ge_2, can be qualitatively described by a modification of the Fermi surface. For UNi_2Si_2, a thermal hysteresis of 4.5 K has been observed in the resistivity anomaly at 53 K, which indicates that the phase transition is of first order.

The two lower phase-transition temperatures of UNi_2Si_2 show a strong field dependence when the magnetic field is applied along the tetragonal c axis. Using the resistivity features at the phase transitions as indicators, a phase diagram has been mapped out through the measurement of resistivity in a magnetic field. An interesting aspect of the phase diagram is the vanishing of the simple body-centred antiferromagnetic phase (AF1) at high fields ($H > 3.5$ T). Such a phenomenon is explained in terms of the energy gain of the LSDW-(C) phase where the net ferromagnetic moments are aligned along the magnetic field.

The temperature dependence of the Hall coefficient of UNi_2Si_2 and UNi_2Ge_2 can be described by the model of Fert and Levy which invokes the magnetic skew scattering of the conduction electrons by the localized moments. For the case of $H \parallel c$ and $I \perp c$, satisfactory agreement with the experimental result is obtained over the entire temperature range measured with a single set of fitting parameters. For the case of $H \perp c$ and $I \parallel c$ however, the experimental data have to be separated into two temperature regions before a satisfactory agreement between the model and the data is obtained. For UNi_2Si_2, the

dividing temperature of the two regions is T_c=53 K. For the case of UNi_2Ge_2, the dividing temperature of the two temperature regions is T_N=77 K. In both cases, the separation is at the magnetic phase transition where an anomalous increase in the resistivity along the c axis occurs. In each of the two compounds, the fitting parameters of the two temperature regions have quite different values, suggesting a profound change in the magnetic scattering potential (R^s) as well as the structure of the Fermi surface (R_H^o) at the magnetic phase transition. The picture of a modified (gapped) Fermi surface is consistent with the description of the resistivity and Hall coefficient. However, it should be emphasized that further investigations (such as optical measurements) are needed before the explanation is on a solid footing.

The temperature dependence of the thermoelectric power of UNi_2Si_2 is not well understood, largely due to the complex nature of the phenomenon itself. Nevertheless, it demonstrates the transport anisotropy of this system. One piece of important information obtained from the thermopower measurements is that the 53 K phase transition has a profound influence upon the electron transport along the c axis, but has very little effect on the electron transport perpendicular the c axis.

The specific heat of UNi_2Si_2 is perhaps the least "abnormal" result measured. The specific heat below 10 K can

be described by a linear term plus a cubic (T^3) term. The extrapolated Debye temperature is 370 K. The γ value extrapolated from the low temperature specific heat is 22 mJ mol^{-1} K^{-2}, which indicates a rather small mass enhancement in the system.

These results of UNi_2Si_2 and UNi_2Ge_2 suggest some new experiments. Optical measurements on both compounds in the far infrared region are of importance because they will provide valuable information about the renormalization of the Fermi surface. It is important to carry out the specific heat measurement on UNi_2Ge_2 to obtain information about the mass enhancement. To clarify the issue of the weak ferromagnetism in UNi_2Ge_2, further susceptibility measurements on high-quality single-crystal UNi_2Ge_2 are needed.

BIBLIOGRAPHY

Alexander S., Helman J. S. and Balberg I. *Phys. Rev B* **13**, 304 (1976)

Amato A., Jaccard D., Sierro J., Haen P., Lejay. and Flouquet J. *J. Low Temp. Phys.* **77**, 195 (1989)

Andersen N. H., Lindelof P. E., Smith H., Splittorff O. and Vogt O. *Phys. Rev. Lett.* **37**, 46 (1976)

Andersen N. H. and Smith H. *Phys. Rev. B* **19**, 384 (1979)

Aschcroft N. W. and Mermin N. D. Solid State Physics, Saunders College, Philadelphia, 1976

Bachmann R., DiSalvo F. J., Jr., Geballe T. H., Greene R. L., Howard R. E., King C. N., Kirsch H. C., Lee K. N., Schwall R. E., Thomas H. U. and Zubeck R. B. *Rev. Sci. Instrum.* **43**, 205 (1972)

Blatt F. J., Schroeder P. A., Foiles C. L. and Greig D. Thermoelectric Power of Metals, Plenum Press, New York, 1976

Chelmicki L., Leciejewicz J., and Zygmunt A. *J. Phys. Chem. Solids* **46** 529 (1985)

Coles B. R. *Contemp. Phys.* **28** 143 (1987)

Collins M. F. Magnetic Critical Scattering, Oxford University Press, London, 1989

Collins M. F. *private communication*, 1991

Dawson A. LeR, Datars W. R., Garrett J. D. and Razavi F. S.

J. Phys: Condens. Matter **1**, 6817 (1989)

Dirkmaat A. J., Ph.D thesis, Leiden University (1989)

Dugdale J. S. The Electrical Properties of Metals and Alloys, Edward Arnold Ltd. London, 1977

Fert A. *J. Phys. F: Metal Phys.* **3**, 2126 (1973)

Fert A. and Hamzic A. in The Hall Effect and Its Applications, Plenum Press, New York, 1980

Fert A. and Levy P. M. *Phys Rev B* **36** 1907 (1987)

Fisher M. E. and Langer J. S. *Phys. Rev Lett.* **20**, 665 (1968)

Geldart D. J. W. and Richard T. G. Dynamical Aspects of Critical Phenomena, edited by J. I. Budnick and M. P. Kawatra, Gordon and Breach, New York, 1972

Grimvall G. The Electron-Phonon Interaction in Metals, North-Holland Publishing Company, Amsterdam, 1981

Gruneisen E. *Ann. Physik* **16, 530 (1933)**

Hurd C. M. The Hall Effect in Metals and Alloys, Plenum Press, New York, 1972

Kittel C. Introduction to Solid State Physics, 5th edition, John Willey & Sons 1976

Kondo J. *Prog. Theor. Phys.* (Kyoto) **32**, 37 (1964)

Lin H. *private communication*, 1990

Lin H., Rebelsky L., Collins M. F., Garrett J. D. and Buyers W. J. L. *Phys. Rev. B* **43**, 13232 (1991)

Lee P. A., Rice T. M., Serene J. M., Sham L. J. and Wilkins J. W. *Comments Cond. Mat. Phys.* **12** 99 (1986)

McElfresh M. W., Rebelsky L., Borges H., Reilly K., Horn S. and Maple M. B. *J. Appl. Phys.* **67** 5218 (1990)

Meaden G. T. Electrical Resistance of Metals, Plenum Press, New York, 1965

Miwa H. *Prog. Theor. Phys.* (Kyoto) **29**, 477 (1963)

Moriya T. in Magnetism (I) Edited by G. T. Rado and H. Suhl, Academic Press, New York, 1963

Ott H. R. *Ann. Rev. Mater. Sci.* **17**, 13 (1987)

Palstra T. T. M. Ph.D thesis, Leiden University, 1986

Palstra T. T. M., Menovsky A. A. and Mydosh J. A. *Phys. Rev. B* **33**, 6527 (1986)

Pines D. and Nozieres P. The Theory of Quantum Liquids, Benjamin, Menlo Park, California, 1966

Richard T. G. and Geldart D. J. W. *Phys. Rev. Lett.* **30**, 290 (1973)

Richard T. G. and Geldart D. J. W. *Phys. Rev. B* 15 1502 (1977)

Schoenes J., Schonenberger C., Franse J. J. M. and Menovsky A. A. *Phys. Rev. B* **35** , 5375 (1987)

Smit J. *Physica* **24**, 39 (1958)

Stewart G. R. *Rev. Mod. Phys.* **56**, 755 (1984)

Suezaki Y. and Mori H. *Prog. Theor. Phys.* (Kyoto) **41**, 1177 (1969)